Department of Chemistry

Synthesis, Surface Assembly, Characterization and Electrochemistry of Gold Nanoparticles

Outi Toikkanen

Aalto University

DOCTORAL DISSERTATIONS

Aalto University publication series
DOCTORAL DISSERTATIONS 19/2011

Synthesis, Surface Assembly, Characterization and Electrochemistry of Gold Nanoparticles

Outi Toikkanen

Doctoral dissertation for the degree of Doctor of Science in Technology to be presented with due permission of the School of Chemical Technology for public examination and debate in Auditorium KE2 (Komppa Auditorium) at the Aalto University School of Chemical Technology (Espoo, Finland) on the 31st of March 2011 at 12 noon.

Aalto University
School of Chemical Technology
Department of Chemistry
Research Group of Physical Chemistry

Supervisor
Professor Kyösti Kontturi

Instructor
Dr. Bernadette Quinn

Preliminary examiners
Professor Hannu Häkkinen, University of Jyväskylä, Finland
Professor Hubert Girault, École Polytechnique Fédérale de Lausanne, Switzerland

Opponent
Professor Robert Whetten, Georgia Institute of Technology, USA

Aalto University publication series
DOCTORAL DISSERTATIONS 19/2011

ISBN 978-952-60-4057-8 (pdf)
ISBN 978-952-60-4056-1 (printed)
ISSN-L 1799-4934
ISSN 1799-4942 (pdf)
ISSN 1799-4934 (printed)

Aalto Print
Helsinki 2011

The dissertation can be read at http://lib.tkk.fi/Diss/

Publication orders (printed book):
julkaisut@aalto.fi

Aalto University

Abstract

Aalto University, P.O. Box 11000, FI-00076 Aalto www.aalto.fi

Author
Outi Toikkanen

Name of the doctoral dissertation
Synthesis, Surface Assembly, Characterization and Electrochemistry of Gold Nanoparticles

Publisher School of Chemical Technology

Unit Department of Chemistry

Series Aalto University publication series DOCTORAL DISSERTATIONS 19/2011

Field of research Physical Chemistry

Manuscript submitted 12.01.2011 **Manuscript revised**

Date of the defence 31.03.2011 **Language** English

☐ **Monograph** ☒ **Article dissertation (summary + original articles)**

Abstract

Gold nanoparticles are intensively studied due to their interesting optical, electronic, catalytic and biological applications. Monolayer protected clusters are particles stabilized by a thiolate layer that have high stability, size-dependent charging behaviour and well established structures. This thesis reports developments in their synthesis and characterization as well as use of electrochemical methods in the field. A synthesis method and full characterization for very small clusters having 38 atoms in their core and a diameter of 1.1 nm is presented. The method is based on the special stability of the Au38 clusters in excess thiol relative to other core sizes formed during the first minutes of the synthesis method used. In this size range, the transition from metallic to molecular behaviour is observed in electrochemical experiments at room temperature. High angle annular dark field - scanning transmission electron microscopy (HAADF-STEM) is used to count the atoms in the cluster core.

Electrochemical methods are used to characterize small clusters as each cluster size has its own charging signature. Electrochemical methods are also used to probe ion permeability of monolayers on nanoparticle surfaces, charging reaction mechanisms and cluster stability. Ion penetration to the monolayer can increase the capacitance and thus the charging energy; this effect can be tuned by the charge of the particle or the properties of the ion and the solvent. Reduction of the Au38 cluster is shown to be irreversible due to desorption of the protecting monolayer. Long-term stability as well as the charge-dependent stability of the Au38 is shown to be solvent dependent. The desorbing species are Au-thiolate oligomers that correlate well with the Au38 structure.

Surface density gradients are structures where the area density of material is continuously varied along the surface. Such structures are of interest in nanotechnology applications in the fields of electronics, sensing and biology. A method for continuously controlling the density of a self-assembled monolayer and nanoparticles attached to it is presented. The molecular area density on the surface is controlled by varying the parameters on electron beam patterning of the self-assembled monolayer, and citrate-stabilized gold nanoparticles are used as labels to visualize the structures.

The results are relevant for fundamental understanding, practical handling and choosing the conditions for applications of gold nanoparticles.

Keywords gold nanoparticle, monolayer protected cluster, synthesis, electrochemistry, surface density gradient

ISBN (printed) 978-952-60-4056-1 **ISBN (pdf)** 978-952-60-4057-8

ISSN-L 1799-4934 **ISSN (printed)** 1799-4934 **ISSN (pdf)** 1799-4942

Pages 136 **Location of publisher** Espoo **Location of printing** Helsinki **Year** 2011

The dissertation can be read at http://lib.tkk.fi/Diss/

Aalto-yliopisto

Tiivistelmä

Aalto-yliopisto, PL 11000, 00076 Aalto www.aalto.fi

Tekijä
Outi Toikkanen

Väitöskirjan nimi
Kultananopartikkelien synteesi, järjestyminen pinnalle, karakterisointi ja sähkökemiallinen tutkiminen

Julkaisija Kemian tekniikan korkeakoulu

Yksikkö Kemian laitos

Sarja Aalto-yliopiston julkaisusarja VÄITÖSKIRJAT 19/2011

Tutkimusala Fysikaalinen kemia

Käsikirjoituksen pvm 12.01.2011 **Korjatun käsikirjoituksen pvm**

Väitöspäivä 31.03.2011 **Kieli** Englanti

☐ **Monografia** ☒ **Yhdistelmäväitöskirja (yhteenveto-osa + erillisartikkelit)**

Tiivistelmä

Kultananopartikkeleita tutkitaan paljon niiden optisten, elektronisten, katalyyttisten ja biologisten ominaisuuksien vuoksi. Yksikerroksella suojatut klusterit ovat tiolikerroksella päällystettyjä partikkeleita. Ne ovat erityisen stabiileja, rakenteet ovat tarkasti määriteltyjä ja sähkökemialliset ominaisuudet koosta riippuvia. Tässä väitöskirjassa kehitetään niiden synteesiä, karakterisointia ja sähkökemiallisten menetelmien käyttöä ominaisuuksien tutkimisessa. Työssä esitellään synteesimenetelmä ja karakterisointi klustereille, jotka sisältävät 38 kulta-atomia ja joiden metalliytimen halkaisija on 1,1 nm. Menetelmä perustuu kyseisen klusterikoon erityiseen stabiilisuuteen ylimäärässä tiolia verrattuna muihin synteesin alkuvaiheessa syntyneisiin klustereihin. Tässä kokoluokassa tapahtuu siirtymä metallisista molekyylinkaltaisiin ominaisuuksiin, mikä voidaan havaita sähkökemiallisilla mittauksilla jo huoneen lämpötilassa. Klusterin ytimessä olevien kulta-atomien lukumäärä voidaan määrittää HAADF-STEM:illa eli pyyhkäisytransmissioelektronimikroskoopilla, jossa kuva muodostuu laajaan kulmaan sironneista elektroneista rengasmaiselle detektorille.

Sähkökemiallisia menetelmiä voidaan käyttää pienten klustereiden karakterisoimiseen, koska jokaisella klusterikoolla on ominainen varautumisvaste. Sähkökemiallisin menetelmin voidaan tutkia stabiilisuutta, reaktiomekanismeja ja pinnalla olevan tiolikerroksen vuorovaikutusta ympäröivien ionien kanssa. Vastakkaismerkkiset ionit voivat tunkeutua nanopartikkelin pinnalla olevaan tiolikerrokseen ja muuttaa sen kapasitanssia ja siten varautumisen energiaa. Vaikutus riippuu partikkelin varauksesta sekä ionin ja liuottimen ominaisuuksista. Au38 klusterin pelkistyminen on irreversiibeli reaktio johtuen suojaavan tiolikerroksen desorptiosta klusterin pinnalta. Stabiilisuus riippuu liuottimesta. Desorboituvat osalajit ovat kulta-tiolaatti-oligomeerejä, mikä vastaa klustereiden tunnettua rakennetta.

Gradienttipinnat ovat pintoja, joissa materiaalin tiheys muuttuu jatkuvasti. Tällaisia rakenteita voidaan käyttää elektroniikassa, sensoreissa ja biologian alalla. Molekyylien ja nanopartikkelien tiheyttä pinnalla voidaan kontrolloida, kun itsejärjestyneellä yksikerroksella päällystettyä pintaa kuvioidaan elektronisäteellä, ja kuvioinnin parametrejä vaihdellaan. Sitraatilla stabiloituja kultapartikkeleita käytetään merkkiaineena molekyylien tiheyden havaitsemiseksi.

Tulokset ovat merkittäviä sekä kultananopartikkelien ominaisuuksien ymmärtämisen että käytännön käsittelyn ja sovelluksiin liittyvien olosuhteiden valinnan kannalta.

Avainsanat kultananopartikkeli, yksikerroksella suojattu klusteri, synteesi, sähkökemia, gradienttipinta

ISBN (painettu) 978-952-60-4056-1 **ISBN (pdf)** 978-952-60-4057-8

ISSN-L 1799-4934 **ISSN (painettu)** 1799-4934 **ISSN (pdf)** 1799-4942

Sivumäärä 136 **Julkaisupaikka** Espoo **Painopaikka** Helsinki **Vuosi** 2011

Luettavissa verkossa osoitteessa http://lib.tkk.fi/Diss/

Preface

The work for this thesis was carried out at the Department of Chemistry, Aalto University in 2006-2011. Academy of Finland and ESPOM graduate school are acknowledged for financial support.

I thank Professor Kyösti Kontturi for introducing the area of electrochemistry, the opportunity for postgraduate studies and constant encouragement. I would like to thank Dr. Bernadette Quinn for the opportunity to work within the fascinating research topic of gold nanoparticles with her and other experts of the field, for a thorough and patient guidance, never-ending ideas, and even when no more working in the lab, always being available and finding time for this work.

I have been lucky to collaborate with excellent researchers throughout the postgraduate work. In the beginning, the people who worked on the topic of gold nanoparticles before me, Dr. Päivi Laaksonen, Dr. Virginia Ruiz, Dr. Timo Laaksonen and Dr. Bernadette Quinn helped me out a great deal in the lab, in getting to know the topic as well as life as a researcher. I want to thank all the collaborators: Ms. Gunilla Rönnholm, Prof. Nisse Kalkkinen and Dr. Amal Dass for collaboration in the mass spectrometry, Dr. Zhiwei Wang and Prof. Richard Palmer in the HAADF-STEM, Dr. Sanna Carlsson in the micropipette measurements and Dr. Peter Liljeroth and Dr. Timo Laaksonen in the modeling. I also thank Prof. Babak Parviz for putting together the research group for the last work, for his ideas and optimism, and the coworkers Mr. Mikhail Erdmanis and Ms. Nguyet Doan who played a crucial role in the success of the work.

My office-mate Lic.Sc.(Tech.) Annukka Santasalo-Aarnio with her positive attitude has been the most important peer support and friend throughout this time in both work and in life's turning points, and for this I want to thank her from the bottom of my heart. All the coworkers at FyKe during this time have played an important role in making the postgraduate time a pleasant experience and I want to thank them all. In particular I want to mention the

"tutors" Dr. Kirsi Yliniemi, Dr. Ben Wilson, Dr. Marjukka Ikonen and Mr. Petri Kanninen who have always been supportive, helpful and have played an important role in me integrating to the scientific community, and Dr. Christoffer Johans, Ms. Nguyet Doan and Ms. Maija Huuppola who also worked in the field of metal nanoparticles and shared their experience.

Working on this thesis project has been considerably less stressful knowing that I have a safety net and source of enjoyment in my life that I can always count on. My warmest thanks belong to all my friends and my large scale family: my husband, parents and my sisters with their families who have encouraged me in the studies, life in general and shared happy relaxed moments that put the life's priorities in the right order.

Outi Toikkanen

Espoo, January 12th, 2011

Contents

List of Publications

This thesis consists of an overview and of the following publications which are referred to in the text by their Roman numerals.

I T. Laaksonen, O. Pelliniemi and B. M. Quinn, Ion Permeability of SAMs on Nanoparticle Surfaces, *J. Am. Chem. Soc.* **128** (2006) 14341.

II O. Toikkanen, V. Ruiz, G. Rönnholm, N. Kalkkinen, P. Liljeroth and B. M. Quinn, Synthesis and Stability of Monolayer-Protected Au38 Clusters, *J. Am. Chem. Soc.* **130** (2008) 11049.

III O. Toikkanen, S. Carlsson, A. Dass, G. Rönnholm, N. Kalkkinen and B. M. Quinn, Solvent-Dependent Stability of Monolayer-Protected Au38 Clusters, *J. Phys. Chem. Lett.* **1** (2010) 32.

IV Z. W. Wang, O. Toikkanen, F. Yin, Z. Y. Li, B. M. Quinn and R. E. Palmer, Counting the Atoms in Supported, Monolayer-Protected Gold Clusters, *J. Am. Chem. Soc.* **132** (2010) 2854.

V O. Toikkanen, N. Doan, M. Erdmanis, H. Lipsanen, K. Kontturi, B. Parviz, Building Molecular Surface Gradients with Electron Beam Lithography, *J. Micromech. Microeng.*, accepted.

Author's contribution

In Publication I, Toikkanen (née Pelliniemi) did nanoparticle synthesis and preliminary electrochemical experiments and participated in preparing the manuscript.

In Publications II and III, Toikkanen optimized the synthesis conditions, prepared the nanoparticles and performed electrochemical measurements (voltammetry, SECM, bulk electrolysis and liquid-liquid interface measurements), and had a major role in planning the experiments and preparing the manuscript.

In Publication IV, Toikkanen was responsible for the nanoparticle synthesis and had an active role in interpreting the results and preparing the manuscript.

In Publication V, Toikkanen was responsible for the nanoparticle and substrate preparations together with N. Doan and had a major role in planning the experiments and preparing the manuscript.

Professor Kyösti Kontturi

Espoo, January 12th, 2011

List of Abbreviations

CB	chlorobenzene
CV	cyclic voltammetry
DCE	1,2-dichloroethane
DCTB	*trans*-2-[3-(4-*tert*-butylphenyl)-2-methyl-2-propenylidene]malononitrile
DFT	density functional theory
DPV	differential pulse voltammetry
E-beam	electron beam
ESI	electrospray ionization
HAADF	high angle annular dark field
HOMO	highest occupied molecular orbital
HR-TEM	high resolution transmission electron microscopy
ITIES	interface between two immiscible electrolyte solutions
LDI	laser desorption-ionization
LUMO	lowest unoccupied molecular orbital
MALDI	matrix-assisted laser desorption-ionization
MP-Au	monolayer protected Au cluster
MPC	monolayer protected cluster
MS	mass spectrometry
NB	nitrobenzene
QRE	quasi-reference electrode
SAM	self-assembled monolayer
SECM	scanning electrochemical microscopy
SEM	scanning electron microscopy
STEM	scanning transmission electron microscopy
STM	scanning tunneling microscopy
SWV	square wave voltammetry
TBA^+	tetrabutylammonium ion
TEA^+	tetraethylammonium ion
TEM	transmission electron microscopy
TGA	thermogravimetric analysis
TOF	time-of-flight
$TPAs^+$	tetraphenylarsonium ion
TPB^-	tetraphenylborate ion
$TPBF_{20}^-$	tetrakis(pentafluorophenyl)borate ion, $[B(C_6F_5)_4]^-$
$TPPA^+$	triphenylphosphoranylidene ion

List of Symbols

a	radius of the particle including the monolayer
a	radius of the microelectrode tip
a_1	location of ion in the monolayer
C	capacitance
c^b	bulk electrolyte concentration
C_{dl}	capacitance of the electrical double layer
C_i	irreversible chemical reaction
C_M	capacitance of the ligand monolayer
C_{MPC}	MPC capacitance
d	monolayer thickness
d	distance of the tip from the substrate in the SECM experiment
e	elementary charge, $1.6021773*10^{-19}$ C
E	potential
E	equivalent number of atoms in HAADF-STEM
E_r	reversible electrochemical reaction
F	Faraday's constant, 96485.31 C/mol
I	current
I_L	limiting current in the SECM experiment
I_{MP}	HAADF intensity of the monolayer-protected cluster
I_{Au38}	HAADF intensity of the size-selected Au38 cluster
k	reaction rate constant
k_B	Boltzmann's constant, $1.380658*10^{-23}$ J/K
K	partition coefficient
L	dimensionless distance in the SECM experiment
m	mass
n	number of electrons
n	exponent in the HAADF-STEM calibration
N	number of atoms
N_A	Avogadro's constant, $6.0221367*10^{23}$ 1/mol
o	organic phase
Q	charge
R	molar gas constant, 8.314510 J/(mol*K)
r_0	MPC core radius
r_g	total radius of the metal tip and glass sheath in the SECM experiment
RG	dimensionless radius in the SECM experiment

r_{ion}	ionic radius
T	temperature
w	aqueous phase
z	MPC charge state
Z	atomic number
α	extent of ion penetration
$\Delta_m^s G$	Gibbs energy of solvation
ΔV	potential difference
$\Delta_o^w \phi$	potential across the water-organic interface
ε_0	vacuum permittivity, $8.85419*10^{-12}$ F/m
ε_m	dielectric constant of the monolayer
ε_s	dielectric constant of the solvent
κ	inverse of Debye length
ρ	charge density
ψ	potential
ψ_0	surface potential

List of Figures

List of Tables

1 Introduction

Nanoscale gold particles have been used in decorative and medical purposes for over two thousand years - well before it was known what caused the extraordinary properties of the materials.[1, 2] The actual science of metal nanoparticles is considered to have started with Faraday's work on their preparation and optical properties in the mid 1800s.[3] Since then, the area has developed through the classical colloid science in the 1900s to today's chemical nanotechnology with precise synthesis methods, well-established structures, advanced characterization methods and applications in the fields of catalysis, electronics and biology.

A key discovery for today's gold nanoparticle science was the use of self-assembly of thiols on gold in nanoparticle stabilization.[4] It resulted in preparation of stable, isolable gold nanoparticles with nowadays precisely known molecular formulas. Gold nanoparticles are the most studied of all metal nanoparticles due to their stability, furthest developed synthesis methods, biocompatibility, interesting optical and electronic properties and best defined electrochemical response.[5] For self assembly of thiols, gold is the most preferred substrate as the gold-thiol bond is very strong.[6] Various functionalities can be added by varying the nature of the thiol. Although bulk gold is well known for being inert, it is an effective catalyst when dispersed in the nanoscale.[2, 7]

This thesis aims to make a contribution to developments in synthesis and surface assembly of gold nanoparticles, their characterization methods and use of electrochemical methods in the field. The first part of the thesis covers synthesis and characterization of gold nanoparticles with emphasis on small thiolate-protected particles having diameters in the order of 1 nm. Synthesis of such small clusters has been a major challenge, and both synthesis methods and understanding of the structures have witnessed significant developments in the past couple of years. Publication II reports a novel synthesis method for small clusters having 38 gold atoms in their cores (Au38) based on their special stability in excess thiol relative to other core

sizes formed during the first minutes of the synthesis. This size range is of great interest as transition from bulk to molecular behaviour has occurred and is observed in electrochemical experiments.

Thiolate-protected gold nanoparticles with diameters smaller than 2 nm demonstrate quantized charging which can be visualized in electrochemical experiments at room temperature. The charging patterns are size-dependent and therefore, electrochemical methods can be applied as a characterization method for small particles. A contribution to resolving the challenges in mass and nuclearity determinations of such small clusters was made by employment of advanced characterization methods, fragmentation-free matrix-assisted laser desorption-ionization time-of-flight (MALDI-TOF) mass spectrometry (Publication III) and high angle annular dark field scanning transmission electron microscopy (HAADF-STEM) (Publication IV).

The second part of the thesis presents the versatile use of advanced electrochemical methods in studying several aspects of thiolate-protected clusters. Besides simple characterization method for small clusters, electrochemical methods can be employed in studying the interaction of the protecting monolayer with the environment by probing the ion permeability of monolayers on nanoparticle surfaces (Publication I), charge and solvent dependent cluster stability (Publication II and III), charging reaction mechanisms and kinetics of electron transfer (Publication II) and degradation products (Publication III).

The third part introduces a novel strategy for patterning self-assembled monolayers (SAMs) with control of the area density of the molecules on the surface (Publication V). Gold nanoparticles are attached to the SAM as labels for electron microscopy imaging. The method is based on variation of the electron beam (e-beam) lithography parameters which allows control of the molecular area density on the surface and therefore, the resulting density of the nanoparticles on the surface. This continuous and tunable density control of molecules and nanoparticles on the surface allows preparation of surface density gradients that are of interest in nanotechnology applications,

systematic study of properties and guidance and growth of biological material (Publication V).

The gold particles used in the studies are so called monolayer protected clusters (MPCs) which consist of a gold core coated with a thiolate monolayer. Publication V is an exception as it presents a more general method for surface density control of nanoparticles. Citrate-stabilized particles were used as labels for visualizing the molecular gradient, but the method is extendable for several types of materials.

Developments in the synthesis methods and surface assembly, stability, characterization methods and understanding the interaction with the medium are important aspects for increasing the fundamental understanding and for successful development of nanomaterials. Potential applications of gold nanoparticles are extremely versatile ranging from energy applications to diagnostics and therapeutics.[2, 8, 9]

2 Gold nanoparticles

This chapter discusses definitions, properties, applications as well as preparation and characterization methods of gold nanoparticles. Preparation methods of gold nanoparticles with the focus in preparing monolayer-protected clusters in the order of 1 nm in diameter are discussed. Characterization methods and cluster structures are introduced. The quantized charging phenomenon is introduced and it is shown how electrochemical methods can be used to characterize the particles based on this phenomenon. A synthesis method for monolayer-protected Au38 clusters and their characterization is presented.

2.1 Background

Nanoparticles belong to the size range between bulk materials and molecules, and this intermediate size can lead to totally new properties which are of interest in novel technology applications. The size range in which new, interesting properties different from bulk behaviour emerge depends on the material and property of interest. Metal nanoparticles usually have diameters below 100 nm, and most of the recent advances have been made in the diameter range below 10 nm.[5]

Nanosized gold has been known for a long time and was originally referred to as colloidal gold. In the 1980s, the term was replaced with the term nanoparticle or cluster following the discovery of the first cluster with a defined molecular formula and narrow dispersity, the so called Schmid's cluster stabilized by phosphane, $Au_{55}(PPh_3)_{12}Cl_6$.[10, 11] The term cluster emphasizes the small number of core atoms and precise molecular composition of the material, and monolayer-protected cluster is used to distinguish liquid-phase prepared, ligand-stabilized clusters from the bare clusters usually prepared in the gas phase by physical methods. The term nanoparticle is commonly used for larger species characterized by diameter, or when generally speaking of different types of species in this size range.

Typical new properties of gold nanoparticles include size-dependent optical, catalytic and electronic properties. Considering electronic applications, an essential property of monolayer-protected gold clusters is their ability to stabilize charge in their cores and act as small capacitors. The phenomenon where electron injection or removal occurs at discrete potential intervals is termed quantized charging and will be discussed in detail in chapter 2.4. The large surface to volume ratio and high amount of surface atoms enhances the catalytic properties of nanoparticles, and nanosized gold is an effective catalyst for a number of reactions[2] as first demonstrated in low-temperature CO oxidation on oxide-supported gold nanoparticles.[7]

The intense colours of gold nanoparticle films or solutions that have fascinated glass and ceramic makers are due to the surface plasmon band, a broad absorption band in the visible region around 520 nm. The surface plasmon band originates from the excitation of collective oscillations of the metallic electrons at the surface of the nanoparticles and is therefore evidence of metallic character. As the core size decreases, the absorption band broadens and its intensity decreases sharply due to loss of metallic character and emerging of quantum size effects.[12] The steplike spectrum typical for small sub-nm particles indicates the transition to discrete energy levels. The plasmon band is also sensitive to the environment which opens the possibility for sensing applications.[1]

Gold is non-toxic and compatible with biological material and therefore suitable for biological applications. Bioconjugates can be prepared through derivatization of the thiolate layer on the nanoparticle. A typical application of gold nanoparticles is labeling biological molecules for electron microscopy. Recently, it was demonstrated that thiolate-coated gold nanoparticles can be used as multivalent therapeutics when conjugated to a fragment of a potent HIV inhibitor.[13] The drug was otherwise inactive but was converted into a biologically active drug by conjugating it to a gold nanoparticle.

2.2 Synthesis

Nanoparticle synthesis in the liquid phase usually begins with reduction of the metal salt leading to nucleation and formation of nanoparticles. To terminate the growth of the particles and prevent their aggregation, the particles need to be coated with a stabilizing layer. A conventional gold nanoparticle synthesis method by Turkevich uses sodium citrate as both reductant and stabilizer and results in water soluble particles with diameters of 15-20 nm.[14] Citrate-stabilized particles are still widely in use due to their straightforward preparation method and excellent visibility in microscopy images. However, they are not stable in dry form and the long-term stability in solution is also limited.

Thiols are known to form a self-assembled monolayer on gold[6] with a strong covalent bond and are therefore an excellent choice as stabilizers. Brust and Schiffrin[4] developed a synthesis method which combined Faraday's two phase reduction method[3] with the self-assembly of thiols on gold and resulted in stable, thiolate-protected gold nanoparticles that can be isolated, redispersed, purified and analytically characterized; in short, they can be handled as simple chemical compounds. The two-phase reduction allows the reduction and surface stabilization to occur simultaneously. In the original preparation method, tetrachloroaurate was transferred from water to toluene using tetraoctylammonium bromide as the phase transfer reagent. Thiol was added to the separated toluene phase and the resulting polymer gold-thiol complex was reduced by slowly adding aqueous sodium borohydride under vigorous stirring. The reaction was allowed to proceed for three hours. The original Brust-Schiffrin method used dodecanethiolate as stabilizing ligand with equimolar amounts of gold and thiol and yielded particles with diameters in the range of 1-3 nm.

2.2.1 Towards smaller clusters

The original Brust-Schiffrin synthesis yields polydisperse material and has to be modified to prepare monodisperse particles of a selected size. Choos-

ing the synthesis conditions involves choice of reduction temperature, reductant addition rate, stirring rate, reaction time, gold to thiol ratio and type of the protecting ligand. In general, the behaviour of the synthesis is consistent with a nucleation-growth-passivation process.[15] Larger thiol to gold ratios, fast reductant addition, low temperature and short reaction time were shown to give smaller average core sizes.[16] For example, a thiol to gold ratio of 1:6 leads to 4.4 nm diameter particles[17] whereas to prepare particles below 2 nm, a ratio of 3:1 is used.[16, 18]

However, when it comes to selective synthesis of clusters containing only a few tens of gold atoms and having diameters in the order of 1 nm, the size cannot be controlled by simply adding more thiol. Preparation methods of such clusters are combinations of tuning the initial synthesis conditions, applying post-synthesis separation steps of different core sizes, or post-synthesis methods that actually change the core size. Post-synthesis separation steps include fractional crystallization, chromatography, solvent fractionation and exposure to excess thiol. Post-synthesis core size evolution can be achieved by etching in neat thiol,[19] heating[20] or ligand-exchange reaction.[21]

The cluster with diameter of 1.1 nm and mass of 8 kDa was first successfully isolated by fractional crystallization from crude mixtures from a synthesis optimized towards smaller clusters and was already then proposed to consist of 38 gold atoms.[16, 22] The molecular behaviour appearing in this size range in optical and electrochemical measurements lead to increased interest in developing synthesis methods that would yield higher quantities of such small clusters. Early synthesis methods for alkanethiolate-protected Au25 clusters (at the time assigned as Au38) required an extremely low reduction temperature of -78 ℃ or 300-fold hyperexcess of thiol.[23] Sterically bulky ligands tend to produce smaller core sizes, and as phenylethanethiol was used as a stabilizer, less extreme conditions were required.[24, 25] The reaction temperature was 0 ℃ and the resulting Au25 clusters could be isolated simply by their solubility in acetonitrile.[24, 25] Another bulky ligand, glutathione, has proven to be an effective protecting agent for the preparation of a wide range of small cluster sizes with a difference of only a few

gold atoms. These water soluble clusters can be separated through electrophoresis and a broad range of core sizes has been reported with 10, 15, 18, 22, 25, 29, 33 and 39 gold atoms.[26] However, due to their water solubility, they are not suitable for electrochemical measurements.[5, 15] Nowadays, most synthesis methods use phenylethanethiol[27-29] or glutathione[29, 30] for preparing Au25 in high yields but also alkanethiols[31-33] can be used. Syntheses are usually either based on the kinetic stability of Au25[27] or its resistance to etching.[30]

Protocols where the synthesis product is exposed to excess thiol have shown to have various outcomes. Exposure to excess thiol can actually change the core size, improve monodispersity or remove unstable core sizes. Core size can be decreased by etching by heating in neat thiol, for example the 14 kDa cluster (nowadays known to have 68 Au atoms[34]) evolved to Au38.[19] Annealing a polydisperse sample with Au144 clusters as the major component in excess thiol in dichloromethane was shown to improve monodispersity.[35, 36] The term annealing was used as distinct from etching, where smaller clusters are formed from larger clusters. In contrast, in the milder annealing process, the procedure was not just etching-based but reduced the proportion of both smaller and larger clusters.[35] This was concluded to be driven by the special stability of the Au144.

However, extraction of Au38 clusters from Au144 clusters by annealing in excess thiol has also been reported[37] and the process will be discussed in detail in chapter 2.5 and Publication II. Chaki *et al*.[33] reported synthesis and isolation for both Au25 and Au38 protected by alkanethiol. Au25 was first isolated based on its solubility in acetone while Au38 and Au144 were isolated based on their stability in neat thiol solution. After the thiol treatment, the Au38 and Au144 clusters were isolated with solvent fractionation.

The mechanisms of the etching or annealing procedures have not been established in detail. An etching mechanism where Au atoms are removed from the cluster surface as soluble Au(I)SR oligomers was proposed based on analysis of the remaining solution after the etching process.[19] In the annealing process,[35] it was suggested that Au atoms are moved between

nanoparticles by Au(I)SR complexes, owing to the fact that Au(I) thiolates can be reactive toward other nanoparticles.[38]

Core size can even evolve during a ligand-exchange-reaction as in a novel synthesis of dodecanethiol or phenylethanethiol-stabilized Au38 clusters prepared by two-phase ligand exchange of glutathione-stabilized polydisperse starting material.[21, 39] This synthesis is very promising as it has higher yields than any previous method and has potential for scale-up.

2.3 Characterization and structures of small clusters

Characterization of very small clusters with only a few tens of atoms in their cores and diameters in the order of 1 nm has been a challenge. While larger nanoparticles are commonly characterized by diameter using transmission electron microscopy (TEM), the smallest clusters cannot be distinguished by diameter even with HR-TEM. The aim in characterization is determining the molecular formula of the cluster, $Au_n(SR)_m$ which is usually reached by mass spectrometry methods.

Early mass spectrometry studies showed that certain cluster masses have extraordinarily high stability.[22] The first studies employed laser desorption-ionization (LDI)[16, 18, 19, 22, 23, 33, 40-44] or matrix-assisted laser desorption-ionization (MALDI)[16, 22, 27, 41, 42] as the ionization method and suffered from fragmentation of the ligands and metal cores. As a result, the detected ions typically corresponded to $Au_nS_m^z$ species. Conclusive determination of the cluster formula was therefore challenging and the core atom numbers were based on assumed geometries giving the so called magic numbers for the clusters with special stability. For example, the Au144 cluster was previously assigned as Au140, 145 or 147, depending on the assumed geometry. The mass percentage of the protecting thiolate layer can be determined using thermogravimetric analysis (TGA), where the material is heated and the fraction of the organic material is detected as mass loss.[45] Many of the first molecular formula assignments have been later corrected as the knowledge of the structures as well as the characterization methods have improved. The

clusters abundantly detected in mass spectrometry studies showing peaks at 5, 8, 14, 22 and 28-29 kDa now have known molecular formulas $Au_{25}(SR)_{18}$,[28, 46] $Au_{38}(SR)_{24}$,[33] $Au_{68}(SR)_{34}$,[34] $Au_{102}(SR)_{44}$[47] and $Au_{144}(SR)_{60}$ / $Au_{146}(SR)_{59}$.[48]

Central breakthroughs in discovering the cluster structures have been electronic structure calculations by density functional theory (DFT) and the total crystal structure determination first reported for $Au_{102}(SR)_{44}$.[47] DFT calculations introduce a divide and protect concept[49] where a gold core is not protected by simple thiolates but ring-like gold-thiolate units and indeed, the crystal structures followed this concept. The structure of $Au_{102}(SR)_{44}$ was refined by electronic structure calculations[50] to consist of a 79-atom gold core with protecting ring-like $Au(SR)_2$ and $Au_2(SR)_3$ oligomers. Both experiment[51, 52] and theory[53] showed that the $Au_{25}(SR)_{18}$ structure was similar consisting of an icosahedral Au13 core protected by $Au_2(SR)_3$ oligomers.

Correlation of optical spectrum and computational studies predicted that $Au_{38}(SR)_{24}$ cluster was also protected by $Au(SR)_2$ and $Au_2(SR)_3$ oligomers.[54] The first complete structure prediction suggested a structure with a bi-icosahedral Au23 core with two face-fused Au13 units and a protecting monolayer of 3 $Au(SR)_2$ and 6 $Au_2(SR)_3$ oligomers.[55] Even a lower-energy isomer was found where the protecting ligands were chirally arranged around the Au23 core[56] and the total crystal structure was determined.[57] The Au144 cluster was proposed to have the molecular formula of $Au_{144}(SR)_{59}$ based on mass spectrometry[33] and the theoretical structure determination gave a formula of $Au_{144}(SR)_{60}$ consisting of a 114 atom core and 30 $Au(SR)_2$ oligomers in the protecting layer.[58] Even higher resolution electrospray ionization mass spectrometry (ESI-MS) showed that in addition to the predicted composition, $Au_{144}(SR)_{60}$, a nearby composition $Au_{146}(SR)_{59}$ was also found in the sample.[48] Relying on the theoretical composition, the cluster is here referred as Au144.

As fragmentation resulted in inaccurate mass and molecular formula determinations, the trend in the field has been to develop a mass spectrometry method that gives the mass of an intact cluster. However, this approach may

still give multiple potential assignments but the best fit with a plausible Au/thiol ratio gives the assignment with high accuracy. Nowadays, fragmentation-free mass spectra are obtained using ESI-MS or fragmentation-free MALDI-TOF mass spectrometry. In ESI-MS, the cluster undergoes ligand exchange for ionisable ligands. The assignment is highly accurate as it is based on analysis of multiple peaks coming from different charge states and degrees of ligand exchange. ESI-MS was already used in the precise distinction of the series of the glutathione-protected clusters having core nuclearities between 10-39[26] and later it revealed that the cluster previously assigned as Au38 was actually an anionic species $Au_{25}(SR)_{18}^-$.[28, 46] Development of fragmentation-free MALDI-TOF mass spectrometry by choice of matrix and conditions has lead to mass determination of an intact cluster.[59]

2.4 Quantized charging

The charging of thiolate-protected clusters is a fascinating phenomenon as it can reflect the transition from metal-like to molecule-like behaviour which is a key feature of nanomaterials. Moreover, these features can be demonstrated in simple electrochemical experiments at room temperature. The ability of metal colloids to accept, store and donate electrons was demonstrated by charging silver or platinum colloids with radiolytically or photolytically generated radicals and using the stored electrons to reduce water to hydrogen.[60, 61] However, only the developments in stabilizing ligands allowed isolation of metal nanoparticles and application of electrochemical methods for studying nanoparticle solutions. Electrochemical studies showed that MPCs are equivalent to diffusing nanoelectrodes in solution[62] and multiple charge states analogous to Coulomb staircase were observed in voltammetry of solution-dispersed Au144 clusters.[63] Size dependence of the charging patterns and transition to molecule-like charging with sub-nm cores was demonstrated.[64] It was demonstrated that charge stored in the MPC core can also be used in redox reactions.[65] Before discussing electrochemical methods for cluster characterization, the quantized charging phenomenon must be introduced.

For metal-like clusters, the charging is a capacitive phenomenon and the successive electron additions or removals are separated by the charging energy only, whereas for molecule-like clusters the charging reflects both the capacitance effect and the discrete, molecule-like energy levels of the cluster. The capacitive charging originates from the combination of nanometer core size and the sub-attofarad capacitance associated with the protecting monolayer. The addition or removal of an electron charges the tiny capacitor and this creates an energy barrier that must be overcome before a second electron can be added or removed.

The additional energy barrier translates into a voltage separation between individual charging events. This can be visualized as waves in cyclic voltammetry (CV) of solution dispersed clusters on a metal electrode or as peaks in differential pulse voltammetry (DPV) or square wave voltammetry (SWV). Several examples of the voltammograms are presented in the following chapters. Each peak corresponds to an addition or removal of an electron, and the peak spacing ΔV is related to cluster capacitance C_{MPC} by $\Delta V = e/C_{\mathrm{MPC}}$.[15, 64, 66] For the experimental observation of quantized charging, ΔV should be greater than $6k_{\mathrm{B}}T/e$ (~150 mV at room temperature) to be able to resolve individual peaks.[67] This is the case with the ubiquitous Au144 cluster with diameter of 1.7 nm whose charging is well reported and up to 15 charge states were observed.[37]

As the core size is further decreased close to 1 nm, such as in the Au38 cluster, the metal-like continuous electron band converts to discrete energy levels analogous to molecular orbitals. Between the highest occupied molecular orbital (HOMO) and lowest unoccupied molecular orbital (LUMO) there is a wide gap, called the HOMO-LUMO -gap, just as in molecules. In electrochemical experiments, the HOMO-LUMO-gap is seen as a large voltage gap between the first electron addition and removal.[64] The first two added or removed electrons occupy the same energy level, and the spacing between them results from the capacitive charging. For such small clusters, the charging is thus a combination of capacitive charging and molecule-like behaviour.

As the cluster capacitance varies with core size and the capacitance is related to peak spacing, monodispersity is an important factor in observing the quantized charging. If the sample is polydisperse, the charging peaks for each size present will overlap.[35] The resulting voltammograms are complicated, with double peaks and shoulders, and the charging peaks for the individual clusters may not be resolvable. As each cluster size has its own charging signature, electrochemical methods provide a direct measure of cluster size and dispersity. For molecule-like particles, the value of the HOMO-LUMO gap is a characteristic feature. The electrochemical HOMO-LUMO gap is corrected for the charging energy to obtain the HOMO-LUMO gap energy, the value of which for example for Au38 is 0.9 eV[37, 64] and for Au25 1.3 eV.[23, 25, 31, 32, 68] There was long confusion in assigning the HOMO-LUMO –gap value to a specific cluster size as both these clusters were assigned Au38. Many reports before 2007 assign the cluster with the 1.3 eV gap determined from optical or electrochemical measurements as Au38,[23-25, 31, 68] but the development of the mass spectrometry methods resolved that this cluster should be assigned Au25.[28, 46] The value of the HOMO-LUMO gap can also be obtained from the optical spectra, where it is seen as the absorbance edge; that is the energy where absorption starts to occur. The electronic excitation in acquiring the optical spectrum does not change the overall charge of the clusters and no correction for charging energy is required.[5]

Stabilizing ligands other than thiolates are rarely used for electrochemical studies of gold nanoparticles. The thiolate ligand used has an effect on the charging in that the dielectric constant of the ligand affects the capacitance of the cluster. If the dielectric constant is too large, discrete charging cannot be resoveld in electrochemical experiments. Therefore, highly polar ligands cannot be used and the electrochemistry of water-soluble clusters cannot be accessed.[5, 15] However, energy levels and single-electron charging of water soluble phosphane-stabilized Au55 clusters were probed by STM of a Langmuir film of Au55 clusters.[69, 70]

In addition to Au144 cluster, quantized charging has been reported to cores having diameters of 2.0 nm (~Au225)[71-74] and 2.2 nm (~Au314).[73] Quan-

tized charging has been reported for other metal cores as well, including Cu,[75] Ag[76] and Pd,[77] but the voltammetric response of gold clusters is much better defined than that of other core metals.

2.4.1 Modeling cluster capacitance

Cluster capacitance determines the charging energy and therefore it is important to account for the parameters influencing the capacitance. Electrostatic models for the charging of the cluster core can predict how the capacitance changes with core diameter and properties of the protecting ligand. The first model used for the cluster capacitance was a purely electrostatic model, the concentric sphere capacitor model:[78]

$$C_{\mathrm{MPC}} = 4\pi\varepsilon_0\varepsilon_{\mathrm{m}}\frac{r_0}{d}(r_0 + d) \qquad (1)$$

where ε_0 is the permittivity of free space, ε_{m} is the dielectric constant of the monolayer, r_0 is the cluster core radius and d is the thickness of the monolayer. The concentric sphere capacitor model does not take into account the electrical double layer formed by electrolyte ions around a charged nanoparticle.[78] It also assumes that all the potential drop between the core and the bulk takes place in the protecting monolayer.[78] Capacitance is taken to be independent of charge state and medium effects are not included.[67] The concentric sphere capacitor model predicts the capacitance well for low charge states and explains the experimentally observed increase in capacitance with shorter ligands and larger cores.[79] The model does not account for the decrease in capacitance at the potential of zero charge which is due to the electrical double layer. Neither does it explain the experimentally observed capacitance changes at higher charge states.[35, 80]

Medium effects were taken into account in the model proposed by Girault *et al.*[81] According to the model, not all the potential drop takes place in the monolayer, but zero potential is reached at a distance far from the particle. The particle is surrounded by the monolayer and the solvent, which have

different permittivity. The peak spacing associated with the capacitance is expressed by equation:

$$\Delta V = \frac{e}{4\pi\varepsilon_0(r_0+d)}\left(\frac{d}{\varepsilon_m r_0}+\frac{1}{\varepsilon_s}\right) \quad (2)$$

where e is elementary charge and ε_s is the dielectric constant of the solvent. The model predicts the solvent dependence of the capacitance but ignores the double layer formation and does not account for charge dependent changes.

To take into account the effect of the electrical double layer, the cluster capacitance is expressed as a sum of the ligand monolayer capacitance, C_M, and the electrical double layer capacitance, C_{dl}:[37]

$$\frac{1}{C_{MPC}} = \frac{1}{C_M} + \frac{1}{C_{dl}} \quad (3)$$

The potential profile in radial coordinates can be calculated by solving the Poisson-Boltzmann equation:[37]

$$\begin{cases} \nabla^2\psi = \dfrac{\rho}{\varepsilon_s\varepsilon_0} = \kappa^2 \sinh\left(\dfrac{F}{RT}\psi\right) \\ \dfrac{\partial}{\partial r}\psi\Big|_{r=a} = -\dfrac{ze}{4\pi\varepsilon_s\varepsilon_0 a^2} \end{cases} \quad (4)$$

where ψ is the potential, ρ is the charge density and a is the size of the particle including the monolayer. κ is the inverse of the Debye-length defined by:

$$\kappa = \sqrt{\frac{2F^2c^b}{\varepsilon_s\varepsilon_0 RT}} \quad (5)$$

where c^b is the bulk concentration of the electrolyte. The Poisson-Boltzmann equation can be solved numerically in two areas: the ligand monolayer and the electrical double layer in the solvent phase. The potential of the nanoparticles is obtained as a function of its charge, Q. The capacitance can be then calculated from the following equation:[37]

$$C = \frac{\partial Q}{\partial \psi_0} \tag{6}$$

This model accounts for the decrease in capacitance at the potential of zero charge, the effect of solvent dielectric constant and the electrolyte concentration. The model assumes that the ligand monolayer is impermeable to electrolyte ions and the effect of electrolyte ions is not taken into account. The variation in capacitance at higher charge states cannot be explained using this model. Refining the model to explain the effect of electrolyte ion penetration to the monolayer is accounted for in Publication I and will be discussed in chapter 3.2 of the thesis. Briefly, the ion penetration is characterized by the distance of closest approach of the electrolyte ions to the core and the increase in capacitance with increasing core size can be explained by the presence of ions in the monolayer.

Another approach to account for the dependence of the charging on the nature of the electrolyte ions was presented.[82] Instead of considering the depth of ion penetration, the ion permeability of the monolayer was characterized by the partition coefficient of the ion between the solution and the monolayer. This method can also account for the capacitance increases with increasing core charge. The model can be solved numerically and the ion penetration is characterized by the partition coefficient K:

$$\nabla^2 \psi = -\frac{Fc^b}{\varepsilon_0 \varepsilon_m}(K_+ e^{-F\psi/RT} - K_- e^{F\psi/RT}) \tag{7}$$

2.5 Synthesis, characterization and properties of hexanethiolate-protected Au38 clusters

2.5.1 Au38 synthesis method

Publication II introduces a novel synthesis method for monodisperse hexanethiolate-protected Au38 clusters. The method is based on the combination of a short reaction time in the synthesis followed by exposure of the particles formed to excess thiol. In the excess thiol treatment, also termed the annealing step, the Au38 core size has a special stability relative to other core sizes formed during the short time synthesis. The inspiration for developing the synthesis method was the fact that short reaction times and low temperatures are generally used to prepare smaller clusters,[16] and the annealing method has been previously used to increase monodispersity.[35, 36] These two approaches were combined here. The reduction time in the Brust-Schiffrin synthesis was optimized such that Au38 were the only clusters that were fully passivated. Larger clusters will not be fully protected by thiolates and are vulnerable to etching in excess thiol. However, from a long-time synthesis, the larger clusters remained stable in the annealing process.

Electrochemical methods were used as the first characterization method of the synthesis products as the charging signature is a good indication of monodispersity and presence of either metal-like or molecule-like clusters. As the reaction time was increased, the voltammetric response of the as-prepared clusters developed towards the characteristic charging signature of Au144 with regular, evenly spaced peaks as shown in Figure 1 a. It is critical for the core size evolution that the synthesis is not stopped for sampling, therefore the results shown here are from separate syntheses. As the short time synthesis product was exposed to excess thiol, the monodispersity improved dramatically towards the pattern with two reduction peaks and four oxidation peaks shown in Figure 1 b. This characteristic charging pattern includes a wide gap of 1.2 V which has previously been assigned to the Au38 core.[37, 64] As the electrochemical gap of 1.2 V is corrected for charging energy, the HOMO-LUMO gap of 0.9 eV is obtained and the same

value is also obtained from the optical spectrum. Au25 was not detected which might be due to the thermodynamic stability of Au38 versus the kinetic stability of Au25.[27, 83]

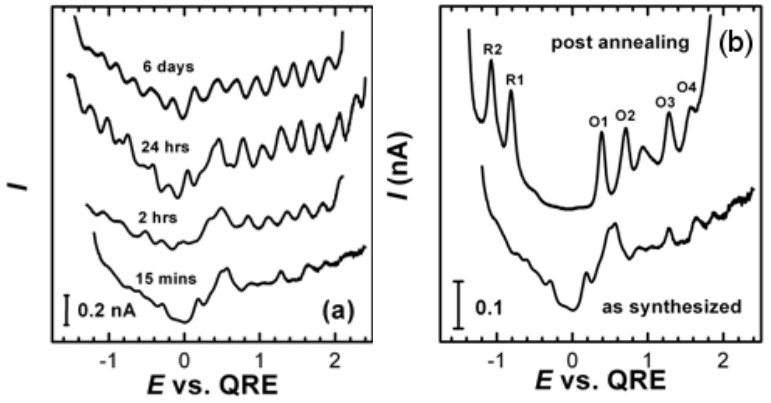

Figure 1. (a) DPVs of the crude synthesis product after the synthesis was allowed to proceed for 15 mins, 2 hrs, 24 hrs or 6 days. (b) DPV of the synthesis product after the shortest reaction time compared with the DPV after the annealing in excess thiol showing the charging pattern characteristic of the Au38 clusters. Reprinted with permission from the American Chemical Society.

In contrast, if the Au144 from a long-time synthesis was exposed to excess thiol, the core size was not reduced, showing that the Au144 is also stable for etching when the reaction time has been long enough for full protection of the core by thiolates. Therefore, the key to the isolation of Au38 with this method is the combination of the short reaction time and annealing.

The absence of additional peaks within the HOMO-LUMO gap in Figure 1 b is an indication of the absence of larger clusters. The additional peaks outside the gap separated by 1.9 V were speculated to originate from smaller clusters based on reported voltammetries for Au11-13 clusters, whose HOMO-LUMO –gap values were in this range.[84, 85] The origin of these peaks is accounted for in greater detail in Publication III and will be discussed together with the stability studies in chapter 3.3 of the thesis.

The correlation of MALDI-TOF mass spectrometry and voltammetry is shown in Figure 2. Even though the mass spectra presented here do not meet

the state-of-the-art standards obtained by fragmentation-free methods, they demonstrate very well how the extra peaks within the HOMO-LUMO gap clearly originate from larger metallic clusters. MALDI-TOF mass spectrometry of the clusters before and after the thiol exposure showed that the additional peaks in voltammetry were due to 22 kDa and 29 kDa clusters which disappeared during the annealing and only the group of peaks at 8.5 kDa remained.

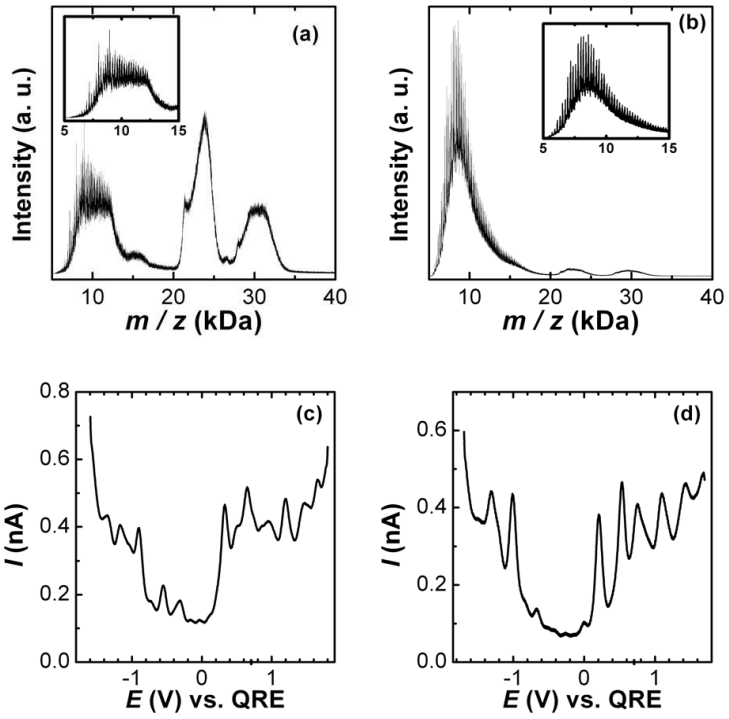

Figure 2. MALDI-TOF mass spectra pre- (a) and post- (b) annealing in excess thiol and the corresponding SWVs pre- (c) and post- (d) annealing. The larger clusters are detected in mass spectrometry at 22 and 29 kDa (a) and as extra peaks within the HOMO-LUMO –gap (c). After the annealing, these peaks in both mass spectrometry (b) and voltammetry (d) almost disappear leaving the group of peaks at 8.5 kDa and the characteristic voltammogram of the Au38 clusters. Reprinted with permission from the American Chemical Society.

Combination of TGA and MALDI-TOF mass spectrometry gave the molecular formula of $Au_{38}(SC_6)_{22}$. In Publication III, MALDI-TOF mass spec-

trometry with optimized conditions was used and the molecular formula was corrected as $Au_{38}(SC_6)_{24}$.

Characterization of small clusters – in this case the Au38 cluster – is a topic that develops throughout the thesis in Publications II-IV. In the first MALDI-TOF mass spectrometry applied for characterization of the Au38 clusters in Publication II, the challenge was fragmentation of the clusters in the ionization process. The first molecular formula $Au_{38}(SC_6)_{22}$ was based on combination of the fragmented mass spectrometry and TGA and was therefore slightly inaccurate. In TGA, any residual thiol or impurity would easily affect the result. Change of matrix and lowering the laser pulse power in MALDI-TOF mass spectrometry lead to a fragmentation-free spectra of thiolate-protected Au25 clusters.[59] The key was to change the matrix from the conventional matrices promoting proton transfer to *trans*-2-[3-(4-*tert*-butylphenyl)-2-methyl-2-propenylidene]malononitrile (DCTB) which promotes electron transfer to the analyte.[59] Use of these parameters in MALDI-TOF mass spectrometry in Publication III resulted in less fragmentation and gave the mass of an intact cluster, but even then the assignment is not absolutely unique. However, the neighbouring assignments can be excluded based on what is a plausible Au/thiol ratio and as a result, the molecular formula $Au_{38}(SC_6)_{24}$ was obtained.

2.5.2 Counting the core atoms by HAADF-STEM

In addition to ESI and fragmentation-free MALDI-TOF mass spectrometries, a method that can be thought as "mass spectrometry on a surface" can be employed for core atom number determination as described in Publication IV. High angle annular dark field – scanning transmission electron microscopy (HAADF-STEM) was used as a method to count the atoms in monolayer protected Au38 clusters using size-selected Au clusters (Au25, Au38 and Au55) as mass standards. The monolayer-protected Au clusters are denoted here as MP-Au38 to distinguish them from the size-selected clusters prepared by sputtering from gas phase.

In DF-STEM imaging, the image is formed by selecting the scattered electrons and therefore, the particles appear bright in the image while the background appears dark. The detector used is an annular detector which surrounds the bright-field detector.[86] HAADF-STEM can be used for imaging really small clusters or even atoms as it uses the electrons diffracted to high angles and the contrast is proportional to Z^n, where Z is the atomic number and the exponent n is calibrated vs. the camera length.

The TEM sample is prepared by drop-casting the cluster solution on the TEM grid and allowing it to dry. Small, monolayer-protected Au clusters (MP-Au) tend to aggregate during drying on the TEM grid as reported previously.[87] Therefore, the HAADF-STEM image of our clusters shows a rather wide size distribution as shown in Figure 3. The larger clusters were shown to be discrete multiples of the smallest clusters (monomers).

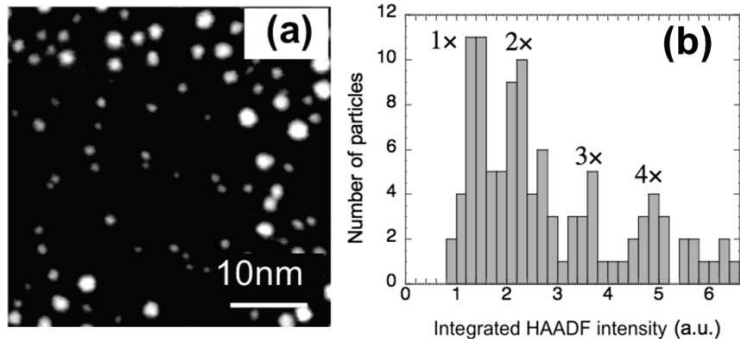

Figure 3. (a) Typical HAADF-STEM image of the MP-Au clusters and (b) histogram of integrated HAADF intensity showing discrete multiples of the smallest clusters. Reprinted with permission from the American Chemical Society.

To determine the number of Au atoms in the monomers, the Au clusters were drop-cast onto the other half of a TEM grid while size-selected clusters were deposited on the other half as shown in Figure 4 a. Figure 4 b and c show typical images for the size-selected Au38 and MP-Au38 clusters, respectively. The monomer MP-Au38 cluster in shown with an arrow, and the shape of the cluster seems to agree with the theoretical prediction.[55] The difference in intensities for size-selected and MP-Au38 shows in Figure 4 d

and e. The intensities of the monolayer-protected gold clusters (I_{MP}) and the size-selected Au38 clusters (I_{Au38}) were compared and the effect of the thiolate ligands was substracted. The peak intensity ratio was measured to be $I_{MP} / I_{Au38} = 1.24$ which gives the equivalent number of Au atoms in the MP-Au monomers $1.24 \times (38.0 \pm 1.0) \approx 47.1 \pm 1.2$. As size-selected Au25 and Au55 clusters were used as mass standards, equivalent numbers of 47.3 ± 1.1 and 46.2 ± 1.2 were obtained, respectively.

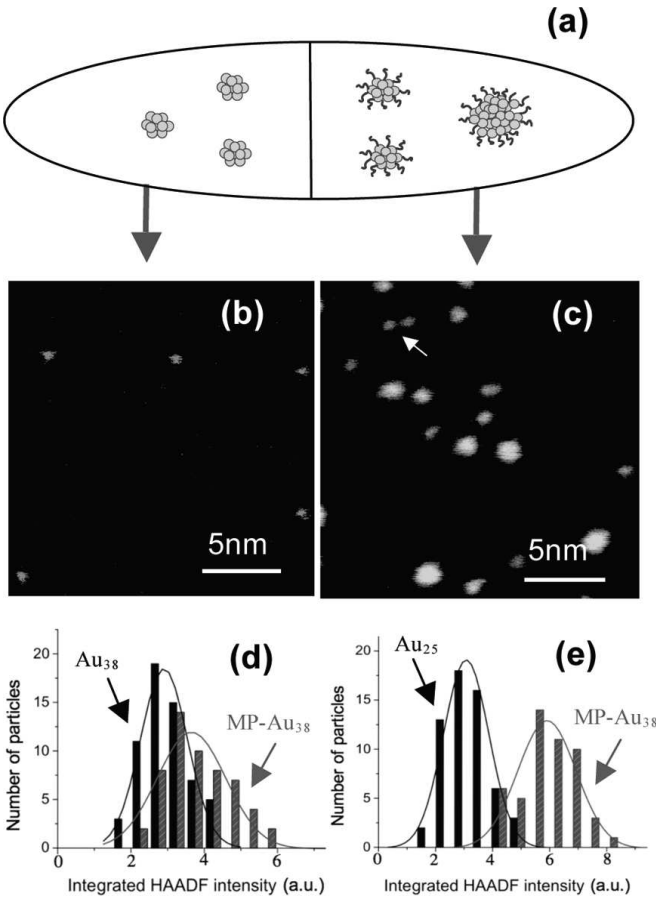

Figure 4. The method to weigh the MP-Au clusters using the size-selected clusters as mass standards: (a) deposition of both cluster types on the same TEM grid. Typical HAADF-STEM images of (b) the size-selected Au38 clusters and (c) the MP-Au38 clusters with the monomer outlined with an arrow. Integrated HAADF intensities of (d) size-selected Au38 clusters and MP-Au monomers and (e) size-selected Au25 clusters and MP-Au monomers. Reprinted with permission from the American Chemical Society.

To substract the effect of the thiolate ligands, the molecular formula $Au_{38}(SC_6H_{13})_{24}$ obtained in Publication III was used. The exponent n was calibrated vs. the camera length (285 mm) and was obtained to be $n = 1.32 \pm 0.12$. Then, the intensity of the S, C, and H in the ligands corresponds to the equivalent number (E) of Au atoms according to the following equation:

$$E = N_S\left(\frac{Z_S}{Z_{Au}}\right)^n + N_C\left(\frac{Z_C}{Z_{Au}}\right)^n + N_H\left(\frac{Z_H}{Z_{Au}}\right)^n \quad (8)$$

Where $N_S = 24$, $N_C = 144$, and $N_H = 312$ denote the number of S, C and H atoms in the molecular formula and $Z_{Au} = 79$, $Z_S = 16$, $Z_C = 6$, and $Z_H = 1$ the atomic numbers. The hexanethiolate ligands are therefore found to contribute an electron intensity signal that is equivalent to 8.7 ± 2.6 Au atoms which is substracted from the equivalent numbers of the MP-Au clusters. The MP-Au clusters are found to contain 38.6 ± 2.8, 38.4 ± 2.9 and 37.5 ± 2.9 atoms when size-selected Au_{25}, Au_{38} and Au_{55} clusters were used as mass balance, respectively. By averaging, the MP-Au monomers were concluded to contain 38 ± 2 Au atoms.

The advantage of the HAADF-STEM determination of the nuclearity is that it discriminates between individual clusters and their aggregates. The aggregation of the clusters on the TEM grid does not disturb the determination. However, the number of thiolates has to be determined with another method before the HAADF-STEM determination can be used for counting the core atoms.

3 Electrochemical studies on monolayer-protected gold clusters

This chapter presents the use of advanced electrochemical methods in studying several aspects of monolayer-protected clusters. In the previous chapter, it was already described how charge states of the thiolate-protected gold clusters can be probed using voltammetric methods and how this can be applied as a characterization method. Peak positions, heights and spacing can give information on the cluster size, monodispersity or interaction with the medium. Voltammetry on macroelectrodes gives information on the reduction and oxidation mechanisms.

Scanning electrochemical microscopy (SECM) was used to obtain more information on the reduction mechanism. Bulk electrolysis was used to probe long-term stability of the oxidized or reduced species. The charged species involved in the degradation of the clusters were detected on a polarisable interface between aqueous and organic electrolyte solutions, and this approach was extended to a generation-collection method where clusters can be charged and the desorbing species can be simultaneously detected.

3.1 Methods

3.1.1 Scanning electrochemical microscopy (SECM)

In scanning electrochemical microscopy, a microelectrode tip with a radius a is moved toward a surface immersed in a solution containing a redox mediator. The tip is biased at such a potential that the redox mediator reacts at the tip and the tip current vs. distance d to the substrate is recorded. The approach of the tip to a conducting substrate gives positive feedback, i.e. the current is higher than in the bulk solution far from the substrate, as the redox mediator is regenerated at the substrate and the diffusion is enhanced close to the substrate. Approach to an insulating substrate gives a negative feedback giving lower current than in the bulk solution due to hindered diffusion

close to the substrate. SECM can be applied for studying the topography, conductivity or reactivity of the substrate surface, the kinetics of the heterogeneous reaction at the electrode surface or homogeneous reactions of products generated at the electrode.[88] Dimensionless parameters used in the analysis are $L = d / a$ and $RG = r_g / a$, where r_g is the total radius of the metal tip and the surrounding glass sheath. The current is normalized versus the current in the bulk solution, I_L.

As the MPCs are known to act as redox species, they can be used as the redox mediator in SECM experiments.[89] Unwin and Bard[90] discussed the application of the feedback mode in studying the rate of the chemical reaction which follows the electrochemical reaction occurring at the tip. Written for a reduction process the reaction scheme is as follows:

$Ox + e^- \rightarrow Red$	at the electrode (E_r)
$Red \xrightarrow{k} P$	following reaction in solution (C_i)

The competitive processes are the diffusion of the Red species to the substrate where it can be regenerated and the decomposition of the Red species to the product, P. If the diffusion time is short compared to the rate of the decomposition, positive feedback is obtained. However, if the kinetics of the chemical step is fast compared to the diffusion, the response will be negative feedback. Between these two extreme cases, the feedback mode can be used for kinetic measurements. This approach is used in Publication II to study the reduction mechanism of the Au38 clusters.

3.1.2 Detection of charged species at the liquid-liquid interface

The interface between two immiscible electrolyte solutions (ITIES) is formed when an aqueous phase containing a hydrophilic electrolyte is brought in contact with an organic phase containing a hydrophobic electrolyte.[88] The liquid-liquid interface is of interest in various electrochemical applications, such as models of biomembranes, ion selective electrodes, in-

dustrial extraction of metal ions as well as electrocatalysis.[88] The interface can be either polarised with no common ion between the phases, or nonpolarised with a fixed potential difference between the phases due to partitioning of common ions.[88, 91] A typical example of a polarised interface is formed between tetrabutylammonium tetraphenylborate (TBATPB) in nitrobenzene (NB) and lithium chloride in water.[88] The electrolytes do not transfer from one phase to another except with high energy, resulting in a large potential window, i.e. an applied potential region where the current due to ion transfer is negligible.

Transfer of charged species across the polarisable liquid-liquid interface can be driven by applying external potential and the transfer event can be detected as a current flow. Ion transfer across the polarisable liquid-liquid measurements is conceptually similar to electron transfer at the electrolyte solution-metal electrode interface in that processes are controlled by mass transfer and Butler-Volmer type kinetics. Thus although the processes are fundamentally different, voltammetric measurements typical of electron transfer studies at metal electrode/solution interfaces can also be used to study ion transfer process at a liquid-liquid interface.[88] Therefore, the polarisable liquid-liquid interface can be used to detect charged species. The liquid-liquid interface can be supported for example at the tip of a micropipette.[92]

3.1.3 Electroanalytical generation-collection method

An electroanalytical generation-collection method for locally generating charged species at a metal electrode and detecting them on a liquid–liquid interface was first introduced by Liljeroth *et al.* for determining the lipophilicity of charged species.[93] The liquid-liquid interface was supported at the tip of a platinum-coated micropipette with the aqueous phase inside the pipette and the organic phase outside. A bipotentiostat was used to control the potential of both the liquid-liquid interface and the Pt coat. This electroanalytical generation-collection method is analogous to the ring-disk electrode experiment, with the Pt coat acting as a generator electrode and the liquid-liquid interface as the detector interface. The micropipette-supported

liquid-liquid interface has an asymmetric diffusion regime: inside the pipette, mass transfer is controlled by linear diffusion while outside it is controlled by spherical diffusion.[92] Therefore, ion transfer from the organic phase to the aqueous phase gives a steady-state wave but gives a peak shaped voltammogram when the ion transfers in the opposite direction. The sign of the current has been defined such that an anion transfer from organic to aqueous phase gives positive current.

The generation-collection method was applied to the study of monolayer-protected gold clusters by Quinn *et al.*[94] Different MPC charge states were generated at the Pt coat electrode and ionic species were simultaneously detected at the liquid-liquid interface. Positive offset current was seen for the as-prepared Au144 clusters having charge state -1. This offset was proportional to concentration and was only removed by increasing core charge. The positive steady-state current response clearly indicates that a hydrophilic anionic species is present in the organic phase with the negatively charged clusters and it was proposed that thiolate desorption occurs from a reduced cluster.

3.2 Ion permeability of the protecting monolayer

Interactions of the thiolate-protected clusters with the environment are essentially interactions of the thiolate layer with the medium. Therefore, the situation under study involves self-assembled monolayers on curved surfaces of nanoscale particles. In Publication I, it was shown that the attractive force between a charged gold cluster and an oppositely charged electrolyte ion can lead to ion penetration into the monolayer. Ions entering the protecting monolayer on a charged gold cluster change its capacitance and thus the charging energy which affects the charging patterns in voltammetric experiments. The extent of penetration can be controlled by MPC charge and properties of the ion and the solvent. The phenomenon was probed on hexanethiolate-protected Au144 clusters (at the time assigned as Au147).

The effects of the electrolyte ions and solvent on the charging properties were studied in voltammetric measurements at a platinum microelectrode. The MPC capacitance, C_{MPC}, is related to the peak spacing, ΔV, in voltammetric measurements by $\Delta V = e/C_{MPC}$. A decrease in peak spacing therefore indicates an increase in capacitance. 1,2-dichloroethane (DCE) and chlorobenzene (CB) were chosen as solvents due to their different dielectric constants, 10.24 for DCE and 5.6 for CB. Electrolyte ions with differing ionic radii were employed: anions PF_6^- and tetrakis(pentafluorophenyl)borate ($TPBF_{20}^-$) and cations tetraethylammonium (TEA^+), tetrabutylammonium (TBA^+), and tetraphenylarsonium ($TPAs^+$). Ionic radii are presented in Table 1. $TPBF_{20}^-$ is a very hydrophobic anion with highly distributed charge. Figure 5 a presents the SWVs for PF_6^- in CB, PF_6^- in DCE and $TPBF_{20}^-$ in DCE focusing on the positive potential region and Figure 5 b for TEA^+, TBA^+ and $TPAs^+$ in DCE on the negative potential region.

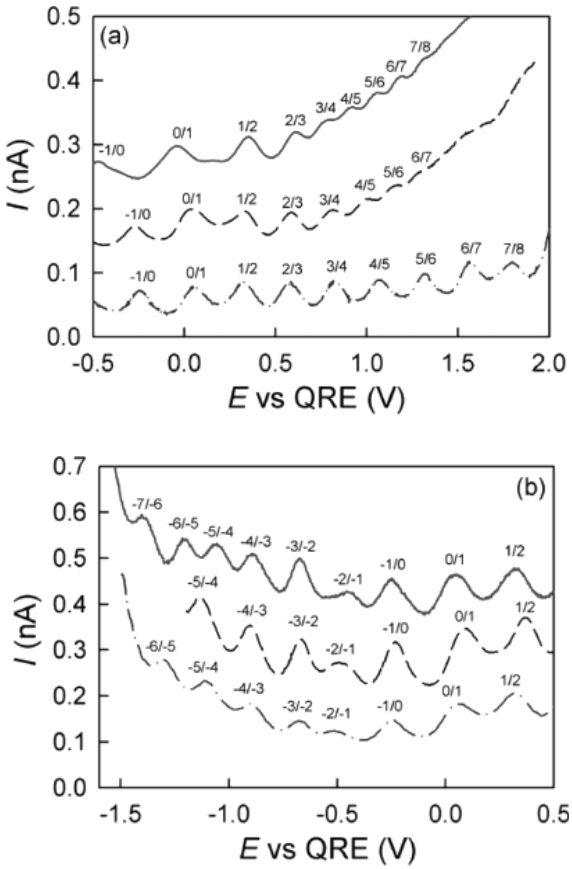

Figure 5. Microelectrode SWVs of MPCs in solution focusing on the positive potential region with (a) PF_6^- as the anion and CB as the solvent showing the largest decrease in peak spacing (solid line), PF_6^- in DCE also showing decrease in peak spacing (dashed) and $TPBF_{20}^-$ with no change in peak spacing (dash-dot), and focusing on the negative potential region in DCE with (b) TEA^+ with most decrease in peak spacing (solid line) and TBA^+ (dashed) and $TPAs^+$ (dash-dot) with comparable decrease in peak spacing. Reprinted with permission from the American Chemical Society.

At zero charge state, the electrolyte ions had no effect in the capacitance. Decreases in peak spacing indicating increases in capacitance were seen for high positive core charges in DCE when the anion was PF_6^-. In this case, changing the solvent to CB enhanced the effect. For negative core charges, TBA^+ and $TPAs^+$ were comparable but the smallest ion TEA^+ caused a more marked decrease in peak spacing.

In this work, the electrical double layer model for calculating the potential profile around the nanoparticle was refined by taking into account the association of a charged nanoparticle and the electrolyte ions. First, the interaction of the charged MPC with electrolyte ions was considered without allowing the electrolyte ions to penetrate the monolayer as shown in Figure 6 a for a negatively charged particle. The potential in three areas was calculated from the Poisson-Boltzmann equation (Eq. 4). Area I denotes the thiolate monolayer, area II is determined by the radius of the specifically adsorbed counterions and area III is the diffuse double layer. The potential profile around the charged nanoparticle calculated using the model with the adsorbed ions was compared with the one obtained from the simple double layer model. The difference between the potential profiles obtained from these models was insignificant and the adsorbed ion model could not reproduce the experimental capacitance changes. Therefore, adsorption alone could not account for the capacitance changes. Next, the model was further modified by allowing the counterions to penetrate the thiolate monolayer as shown in Figure 6 b for a positively charged particle. The potential was again calculated in three areas, area I now being the ion-free monolayer, area II the part of the monolayer where ions are present and area III is the diffuse double layer.

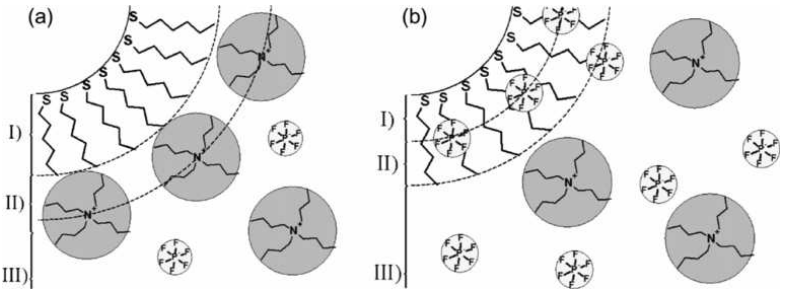

Figure 6. Ion distributions around (a) a negatively charged MPC with specific adsorption of the counterions, where area I is the thiol monolayer, area II is the distance of closest approach for the counterion and area III is the diffuse double layer and (b) a positively charged MPC with penetration of the counterions into the monolayer, area I now being the ion-free monolayer, area II the part of the monolayer where ions are present and area II the diffuse double layer. Reprinted with permission from the American Chemical Society.

The extent of ion penetration α is defined as

$$\alpha = \frac{a_1 - r_0}{d} \tag{9}$$

where a_1 is the location of the penetrating ion in the monolayer, r_0 is the MPC core radius and d is the monolayer thickness. α has values between 0 and 1, 1 meaning that no penetration occurs. The extent of penetration was varied to get a fit between the theory and experiment. The results are summarized in Table 1. All the cations penetrated the monolayer when the MPC charge was negative, with TEA^+ penetrating most (α = 0.49). For PF_6^- in DCE, the best fit was obtained by allowing α to gradually change from 1.0 to 0.6 with increasing charge. With the same ion in CB, α was kept close to 0.9 for the first two charge states and then let drop to 0.44. $TPBF_{20}^-$ did not penetrate the monolayer at all.

Table 1. Extent of ion penetration (α) obtained from the fitting, calculated distance of the ion from the core surface (a_1-r_0) and ionic radii used in the fitting.

	α	$a_1 - r_0$ / Å	r_{ion} / Å
PF_6^- (CB)	0.9 – 0.44	6.9 – 3.4	1.4
PF_6^- (DCE)	1 – 0.6	7.7 – 4.6	1.4
TEA^+ (DCE)	0.49	3.8	3.4
TBA^+ (DCE)	0.74	5.7	4.1
$TPAs^+$ (DCE)	0.7	5.4	4.3
$TPBF_{20}^-$ (DCE)	1	7.7	4.2

The effect of the solvent can be rationalized by considering the energetics of ion solvation in the monolayer relative to bulk solvent. The difference in the Gibbs energy of solvation can be estimated using the Born model

$$\Delta_m^s G = -\frac{N_A z^2 e^2}{8\pi\varepsilon_0 r_{ion}}\left(\frac{1}{\varepsilon_s} - \frac{1}{\varepsilon_m}\right) \tag{10}$$

It can be concluded that less energy is required to transfer the ion from bulk solvent to the monolayer when the dielectric constant of the solvent is closer to that of the monolayer.

3.3 Stability and reaction mechanisms of Au38

Stability of the thiolate-protected gold clusters is essentially related to the stability of the protecting monolayer. Based on macroelectrode voltammetries, the reduction and oxidation mechanisms of thiolate protected Au25 clusters are known to be different: the oxidation is a reversible one-electron transfer reaction whereas the reduction consists of successive electrochemical and chemical steps where the cluster reduction is followed by desorption of a negatively charged thiolate species, and the neutral cluster can accept another electron at the same potential.[68] Reductive desorption of thiolates from planar gold surfaces is well established[95] and is known to be a one electron transfer reaction, the desorbing species being a thiolate anion. The process is reversible: if the negative potential applied on the gold surface is switched off the desorbed thiolates can be readsorbed.[96] The connection between the thiolate desorption and cluster stability has prevented the study of thiolate desorption from small clusters.

Charge dependent stability was probed using cyclic voltammetry and bulk electrolysis (Publication II). More information on the mechanisms of the charging reactions was obtained by scanning electrochemical microscopy (SECM). In Publication III, solvent dependent stability was studied, and the electroanalytical generation-collection method described in the previous chapter was applied for studying charge dependent stability.

3.3.1 Charge dependent stability

In light of the structure of the clusters, probing the influence of charge on the stability is an interesting aspect. Based on voltammetries on both micro- and macroelectrodes (Figure 7 a), it is clear that the reduced particles are not as stable as their oxidized counterparts.

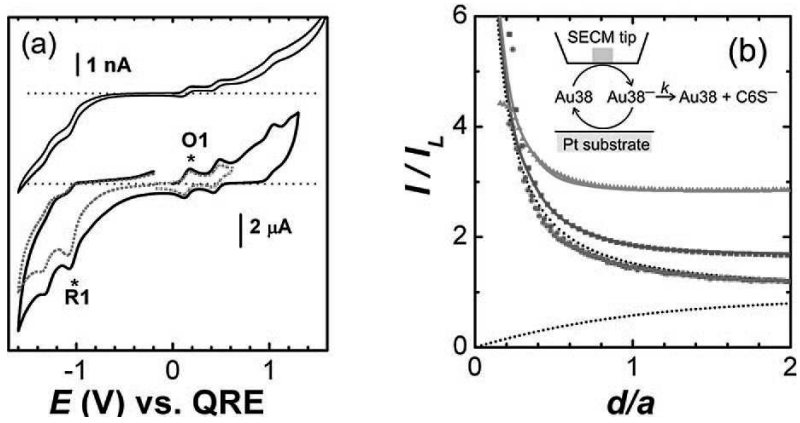

Figure 7. (a) CVs of Au38 at a Pt microelectrode (upper trace) and macroelectrode (lower trace). The dotted lines are single scans for oxidation and reduction and the first oxidation (O1) and reduction (R1) peaks are marked with asterices. (b) The SECM approach curves from top to bottom, the dots showing the experimental data and the solid lines the fitted curves: for Au38 reduction to -1 with the tip radius 12.5 µm, for Au 38 reduction to -1 with the tip radius 5 µm, and for Au38 oxidation for tip radii 5 µm and 12.5 µm (the lowest overlapping traces). The dotted lines show ideal negative and positive feedback. Reprinted with permission from the American Chemical Society.

CVs on macroelectrode show that the oxidation is a simple one-electron diffusion-limited reaction as it gives Nernstian peaks for both forward and reverse scans that scale with scan rate. The reduction is clearly more complicated. The reverse scan peaks are completely absent for low scan rates indicating that the reduced species is no longer available to be oxidized. For both micro- and macroelectrodes, the reduction peak currents are significantly greater than those for oxidation indicating that more that one electron is transferred at the same potential. This was explained by a cascade reaction consisting of electrochemical and chemical steps, denoted as the $(EC)_n$ mechanism, where the reduction of the cluster is followed by desorption of negative thiolate species from the protecting layer. The desorption results in a neutral cluster which can again accept an electron at the same potential. The reaction scheme is written here using the first molecular formula $Au_{38}(SC_6)_{22}$ later corrected to be $Au_{38}(SC_6)_{24}$:

$Au_{38}(SC_6)_{22} + e^- \rightarrow Au_{38}(SC_6)_{22}^-$ (E)

$Au_{38}(SC_6)_{22}^- \rightarrow Au_{38}(SC_6)_{21} + C_6S^-$ (C)

$Au_{38}(SC_6)_{21} + e^- \rightarrow Au_{38}(SC_6)_{21}^-$ (E)

and so on. The desorbing species is here denoted as simple thiolate but is likely to be a more complicated Au-thiolate species in light of the structure determinations. The reaction is characterized by the rate constant of the chemical step, *k*, and the total number of electrons accepted, *n*. The electron transfer reactions are assumed to be fast and have the same standard potential. From simulated CVs, it can be concluded that *n* is larger than 2 or 3, but the stability of the clusters requires that it cannot be larger than ~10. Bulk electrolysis and two-phase oxidation experiments also showed that the clusters were stable over oxidation as the voltammetry features were sustained after the oxidation. In contrast, as the clusters were reduced by bulk electrolysis, the characteristic peaks in the voltammetry were lost.

More information on the mechanism was obtained by using the clusters as redox mediators in SECM experiments as illustrated in the inset of Figure 7 b for the reduction reaction followed by the homogeneous chemical reaction. Different Au38 charge states were generated on the tip by applying potentials selected from the voltammograms recorded at the tip. Approach curves were measured by monitoring the diffusion-limited tip current as a function of the distance from the Pt substrate. If the redox mediator is undergoing reversible reaction and is regenerated on the conducting substrate, the current close to the substrate is higher than in the bulk and pure positive feedback is obtained. Approach curves to Pt substrate for z = +1 and +2 gave pure positive feedback, but for z = -1 and -2, there was deviation from ideal positive feedback (Figure 7 b). The larger tip (a = 12.5 µm) showed more deviation as the smaller one (a = 5 µm). In the case of the smaller tip, the reduced cluster will reach the substrate before the following reaction will occur. The SECM mechanism was modeled according to the $(EC)_n$ mechanism and fitted better to the limit of large n than to n = 2, 3 or 4. The rate constant of the homogeneous step was obtained to be 8 s^{-1}.

3.3.2 Solvent dependent stability

In Publication III, it was demonstrated that the stability of the Au38 clusters in solution is critically solvent dependent. Long term stability in solution was probed by following the development of the voltammetry response on a microelectrode and using the liquid-liquid interface supported on a tip of a micropipette for detection of ionic species in solution. In chlorobenzene, the voltammograms remained unchanged as shown in Figure 8 a indicating that the clusters were stable over long periods of time. In dichloroethane (Figure 8 c), the degradation of the Au38 clusters was seen as gradual disappearance of the characteristic peaks, and only the impurity peaks remained. The voltammogram of the remained solution was similar to that previously assigned as Au11-13,[84, 85] but no clusters were detected in that mass range (2-3 kDa) in fragmentation-free MALDI-TOF mass spectrometry of the initial solution or LDI-TOF mass spectrometry of the degraded solution. Instead, enhanced amount of peaks were detected in LDI-TOF mass spectrometry below 1 kDa that were identified as Au-thiolate oligomers. Peaks at this region are present also in LDI-TOF mass spectra of the cluster solution due to fragmentation of the clusters, but here there are no larger clusters that could be fragmented, and the peaks can only be ascribed to the degradation products. The peaks that could be identified correspond to species with one gold atom AuS_2, AuSR, AuS(SR), $Au(SR)_2$, two gold atoms $Au_2S(SR)_2$, Au_2SR_3 or even three gold atoms $Au_3S(SR)$, but oligomers containing more than 3 Au atoms could be excluded. The result is in line with the Au38 structure that is known to include a gold core protected with ring-like $Au(SR)_2$ and $Au_2(SR)_3$ units.[55, 56]

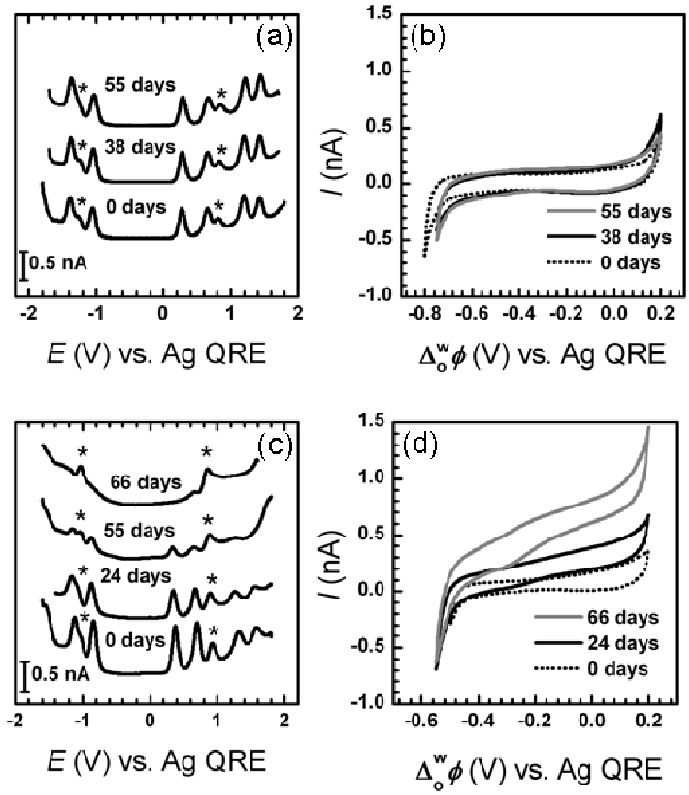

Figure 8. Microelectrode SWVs for Au38 recorded over a period of time dispersed in (a) CB and (c) DCE and the corresponding CVs recorded at the liquid-liquid interface supported at the tip of a micropipette in (b) CB and (d) DCE. The impurity peaks are marked with asterices in (a) and (c). Reprinted with permission from the American Chemical Society.

The electrified liquid-liquid interface was used to probe the species in solution. For chlorobenzene, the CV at the liquid-liquid interface remained unchanged as shown in Figure 8 b, in line with the microelectrode voltammetry. In contrast, for dichloroethane, a positive current offset becomes apparent over time as shown in Figure 8 d. This offset can only be due to anionic species transferring from the organic to the aqueous phase.

Correlating the mass spectrometry data with the microelectrode and micropipette voltammograms, it can be concluded that the impurity peaks in the SWVs are due to Au- thiolate oligomers. However, they cannot be directly

correlated to the species detected on the w/DCE interface. As they were apparent even in CB while no ionic species were detected on the interface, it is concluded that there are two kinds of Au-thiolate species in the solution. The other ones are initially present in solution and are either uncharged or relatively hydrophobic and are visualized as the additional peaks in the SWV, while the other ones are formed during degradation. The species from cluster degradation detected at the w/DCE interface are both anionic and hydrophilic.

Next, the role of the solvent in charge dependent stability of the clusters was studied using the generation-collection method described earlier. Different cluster charge states were generated on the Pt coat electrode, while the charged species were detected on the water-organic interface on the micropipette. The charged clusters themselves do not transfer across the interface and any increase in current can be assigned as transfer of ionic species desorbed from the charged cluster. In the case of CB, there is a slight offset current, while for DCE, the current offset is marked indicating that also when reduced, the clusters are more stable in CB than DCE. The current offset increased with the Au38 charge number indicating enhanced desorption as a function of charge state. Desorption of the charged species as the clusters are reduced is not unanticipated based on the literature, but the extent of desorption dependence on the solvent is unexpected.

The role of the solvent was also considered in the annealing process that is an important step in the Au38 synthesis. Annealing the short time synthesis product in DCE in the presence of excess thiol effectively removes the larger clusters and yields highly monodisperse Au38 clusters. However, the same procedure in CB results in polydisperse material where at least two core sizes, Au38 and Au144, are present. In conclusion, Au38 has no special stability compared to other core sizes in CB when excess thiol is added, but is stable over other core sizes in DCE under the same conditions. Without the excess thiol addition, the Au38 degrades in DCE but keeps its stability in CB.

The results point a strong role of the solvent in the stability of MPCs both in long-term storage and in charge-dependent behaviour. The origin of the effect may be the nature of the protecting monolayer and its coordination with the solvent. Au MPCs cannot be handled without solvent dispersion. Solvent plays a critical role in preparation, purification, characterization, electrochemistry, surface functionalization and shelf-life of MPCs. It is also essential for the formation of nanoparticle superstructures. It may account for the controversies in the different post-synthesis treatments to prepare small gold clusters. The results presented in Publication III are relevant not just for fundamental understanding of the properties of Au MPCs but also for all practical treatment of such compounds.

4 Surface density gradients of gold nanoparticles

Attachment of nanoparticles on surfaces and patterning surfaces with nanoscale features are an essential part of nanotechnology. This chapter introduces methods to control the area density of nanoparticles on surfaces. Nanoparticle density control often equals to controlling the area density of the molecules that are used to attach nanoparticles on surfaces. Controlling the density of those linker molecules is often achieved by modification of SAMs. Here, the focus is on methods that have potential for continuous variation of density on tunable scale areas, so called gradient preparation.

4.1 Background

Controlled assembly of nanoparticles is essential in many nanotechnology applications such as electronic and optical devices, sensors or interaction of nanoparticles and biological material.[1] The ability to control the area density of molecules or particles on the surface in a continuous and tunable fashion allows preparation of surface density gradient structures. Surfaces with chemical concentration gradients are of wide interest in science because they allow systematic study of properties as a function of surface density, and an entire spectrum of properties can be studied on a single surface.[97-100] Such structures could be useful for systematic property optimization for applications as catalyst materials, sensors, filters, attachment of further molecules and interaction of nanoparticles and biological material.[98] Gradient preparation is also motivated by their ability to drive transport phenomena, for example a hydrophobicity gradient was used to transport a drop of water uphill on a surface,[101] and many biological species respond to concentration gradients. Cells can move according to concentration gradients, and growth of neurons has been guided by proteins attached on a nanoparticle gradient on surface.[102] Considering the types of phenomena gradients can drive in the larger scale, it is intriguing to explore the potential of such structures in the nanoscale.

Nanoparticles are usually attached on surfaces by first forming a self-assembled monolayer of molecules which can then attract the nanoparticles. The most common attachment strategies utilize the thiol bonding onto a metal surface or silane bonding to the hydroxyl groups on the surface of glass or silicon. Thiol or amino functionality on the other end of the molecule is commonly used to attach the nanoparticles on the surface. Amino-terminated molecules are active for attachment of several types of material through peptide bond formation, electrostatic attraction in acidic media or the affinity of the amino group to metals. In acidic media, the amino group is protonated and can attract negatively charged particles such as citrate-stabilized metal nanoparticles.[103]

Here, the focus is on methods that have potential for SAM/nanoparticle gradient preparation. Gradients can show functionality as 1D, 2D or 3D structures, although a true 1D gradient has not yet been reported. Whether the density is continuous or not depends on the scale at which we are looking the structures. Most surface gradients are not continuous in the molecular level but in a larger scale can be considered as gradients.

Deposition of metal nanoparticles on selected areas of the substrate can be directed by starting with a lithography step after which the particles are attached to patterned surfaces. Alternatively, patterns of metal nanoparticles can be printed on surfaces using microcontact printing or arranged atom by atom by STM writing. Nanoparticle gradient preparation can begin with forming a gradient of the linker molecules followed by nanoparticle attachment, or by forming a gradient of the nanoparticles on a homogeneous SAM. Gradient SAM preparation can include top down modification of a homogeneous substrate, or bottom up steps where the material is gradually deposited on the surface. Several methods have been reported for SAM gradient fabrication in the macroscale and there is increasing interest in development of methods with potential to scale down.[99] Macroscale gradients can be prepared by gradually changing the immersion time in solution,[104, 105] vapor diffusion[101] or thermochemical manipulation of the SAM.[106] Methods with potential to scale down include vapor diffusion on flexible sub-

strates,[107] gradual contact printing,[108] edge-spreading lithography[109] and STM-based replacement lithography.[110]

Densities and interparticle distances of citrate-stabilized gold particles on amino-terminated surfaces can be controlled by ionic strength or pH but continuous gradients of such particles in nanoscale areas have not been reported.[111, 112] Physical low-energy cluster beam deposition process has been used for creating a cluster gradient with nanoscale steepness and dimensions but the number density gradient was coupled with gradient in particle size.[113]

Electron beam (e-beam) lithography is a versatile tool for patterning as it has a wide flexibility for size range and the e-beam dose and acceleration voltage can be varied. The state-of-the-art semiconductor manufacturing tools use e-beams to pattern with better than 10 nm resolution over areas extending more than 10 cm in length. E-beam lithography has been used for direct patterning of nanoparticle films[114] or self-assembled thiolate or silane monolayers.[115-122] E-beam exposure of SAMs can have various effects: removal, partial removal, disordering, dehydrogenation, crosslinking or change of functional group.[119, 120, 122] The nature of the SAM determines the response to e-beam exposure as exposed aliphatic SAMs become soluble and act as positive resists whereas aromatic ones become insoluble and in turn act as negative resists. E-beam can even change the chemistry of the surface as reported by Mendes and coworkers who changed the surface group functionality from nitro to amino allowing the attachment of gold nanoparticles.[119]

Low-energy patterning of amino-functionalized silane layer has been shown to result in removal of the amino group while the carbon chain remained intact, and palladium colloids were attached on the unexposed areas where the amino groups were still available for attachment.[115] Electron irradiation has been used to facilitate the thiolate exchange reaction on gold surface, and the extent of the exchange could be controlled by varying the dose.[123, 124] Combined with e-beam lithography, this technique could be used for functional thiolate gradient fabrication.

4.2 Molecular surface gradients with electron beam lithography

Despite the large variety of density control and patterning methods available, few of them allow tunable, continuous variation of the nanoparticle densities on different areas of the surface. Publication V presents a method for preparing such metal nanoparticle gradients in small scale areas on surfaces. The silicon surface is first modified with an aminosilane layer where the nanoparticles can be attached. Subsequently, the silane layer is patterned using e-beam lithography followed by immersion in citrate-stabilized gold nanoparticle solutions in acidic pH. The patterning strategy is illustrated in Figure 9. This fabrication method can be used for gradient preparation as the e-beam parameters can be varied to control the amount of linker molecules etched and therefore, the density of nanoparticles on the surface. The patterns on silane layer as well as the nanoparticle arrays were imaged by scanning electron microscopy (SEM). The nanoparticle density dependence on the e-beam dose at different acceleration voltages was established and continuous surface density gradients of differing steepness were prepared.

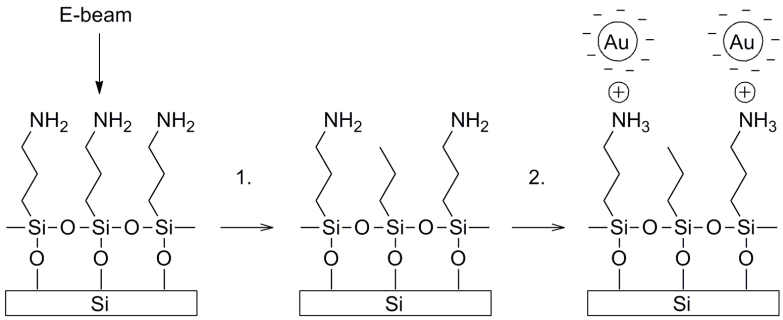

Figure 9. Schematic of the gradient preparation strategy: (1) E-beam exposure of the aminosilane-SAM alters the density of functional amino groups on the surface. Applied dose controls the effective area density. (2) Negatively-charged gold nanoparticles are attached to the remaining amino groups in acidic conditions. Reprinted with permission from the Institute of Physics.

The patterns on the amino-functionalized silicon were visible in the SEM images even before the nanoparticle attachment. The effect of the dose

shows as a fading contrast as the dose decreases as shown in Figure 10 a where the dose decreases on each line from right to left. The density-dose dependence was determined by treating different areas of the substrate with e-beam varying the acceleration voltage and dose. For each voltage, a set of lines with varying e-beam doses was written on the substrate and the density-dose dependence was established at each voltage. Larger dose always resulted in lower density of nanoparticles, which is explained by a dose-dependent modification of the silane layer. After exposure with larger dose, there will be less amino groups available for attachment, and the resulting nanoparticle density is lower. However, the density vs. dose dependence is dependent on the acceleration voltage. At 1 kV, the particle density never dropped close to zero. At the voltages 3-12 kV, the lower the voltage, the lower the dose to needed to modify the silanes.

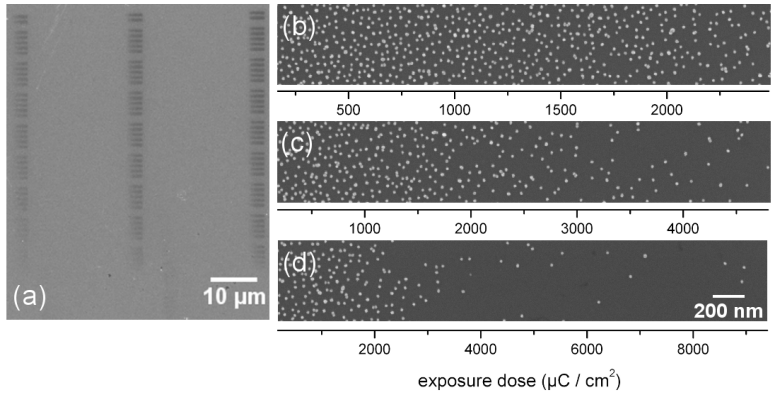

Figure 10. (a) SEM image of gradient lines written with acceleration voltage of 3 kV on an amino-functionalized silicon surface before the nanoparticle attachment. (b-d) SEM images of nanoparticle density gradients with varying densities and steepness. The acceleration voltage was 3 kV and the dose ranges were (b) 160-2480 µC / cm^2, (c) 160-4800 µC / cm^2 and (d) 160-9440 µC / cm^2. The 200 nm scale bar applies to all images (b-d), and the exposure dose axis illustrates the dose in each position of the sample. Reprinted with permission from the Institute of Physics.

The gradient patterns were prepared by gradually changing the dose along the pattern. Examples of nanoparticle gradients of different steepness are shown in Figure 10 b-c. The gradients consist of 30-nm-long subareas where the dose is constant, and for the next subarea, the dose is increased by

a dose step value. The minimum and maximum doses control the nanoparticle densities at each end of the gradient line, and the dose step value controls the gradient steepness.

The lines prepared using lower voltages have sharper boundaries as also reported previously.[115] With higher acceleration voltage, the beam penetration area increases resulting in backscattered electrons. The exposure time required to prepare the gradients was of the same order for all voltages. The increase in exposure dose was mostly compensated by the increase in the current flowing to the specimen. To prepare a gradient of our chosen geometries and materials, it is beneficial to use the voltage 3 kV as it has the maximum flexibility in density and the best pattern quality.

The patterning strategy for an amino-terminated silane layer has a great potential for variation. The amino group can be attached to several types of metal or polymer nanoparticles, carbon nanotubes, fluorescent quantum dots or biological material. Silanes can bond to glass which allows optical characterization and applications. Conductive indium-tin oxide glass is suitable for e-beam substrate and could be used for electrode or sensor applications. The method is not even restricted to aminosilane on silicon and citrate-stabilized gold particles, but has potential for surface density control and gradient preparation for various types of substrates, SAMs and materials attached to the SAM. However, the parameters for gradient preparation have to be optimized according to the materials and preparation methods.

5 Summary

This thesis reported developments in monolayer protected gold cluster synthesis, their characterization methods, organization of nanoparticles on surfaces and use of electrochemical methods in studying various aspects of monolayer-protected clusters.

A synthesis strategy for thiolate-protected gold clusters having 38 atoms in their cores was presented. The strategy is based on exposing a short time synthesis product to excess thiol. In the short time synthesis, the Au38 is the only cluster size that is fully protected by thiolates, and larger core sizes can be removed by etching in excess thiol. The cluster has a molecular formula of $Au_{38}(SR)_{24}$, core diameter of 1.1 nm and HOMO-LUMO gap of 0.9 eV as determined from optical and electrochemical measurements. The mass of an intact cluster obtained using fragmentation-free MALDI-TOF mass spectrometry was 10.3 kDa. Previously, using mass spectrometry which still suffered from fragmentation, the Au38 cluster was detected at 8.5 kDa as the carbon chains were removed under the ionization process. HAADF-STEM can be used for calculating the atoms in the cluster core if the number of thiolates is known, and the core atom number 38 ± 2 was obtained.

Electrochemical methods can be used as a simple cluster characterization tool, as each cluster size has its own charging signature. Oxidation and reduction reactions of the clusters were studied by cyclic voltammetry and scanning electrochemical microscopy. It was revealed that oxidation is a simple, reversible one-electron transfer, but reduction is an irreversible process with more electrons transferring at the same potential. A reduction mechanism was formulated where the reduction step is followed by desorption of anionic species, and the neutral cluster can again accept an electron at the same potential. As the stability of the clusters depends on the stability of the thiolate monolayer, reduced clusters are not stable but desorption of the thiolate species results in irreversible aggregation.

Long-term stability of the clusters was shown to be solvent dependent. The clusters were stable indefinitely when the solvent was chlorobenzene, but degraded over a period of weeks in 1,2-dichloroethane. Voltammetry studies at a microelectrode and a liquid-liquid interface as well as mass spectrometry showed that the loss of characteristic charging peaks were related to detection of anionic species at the liquid-liquid interface and in mass spectrometry. The remaining peaks in voltammetry were associated with Au-thiolate oligomers containing less than three Au atoms, in line with the Au38 structure.

Solvent was shown to play a role even in the charge dependent stability of the clusters. Desorption of the anionic species was increasing as the clusters were reduced and this effect was far greater in DCE than in CB. Solvent also had a critical role in the annealing method included in the extraction of the Au38 clusters in excess thiol. If the annealing step was carried out in CB, Au38 had no special stability relative to other core sizes, therefore, it is critical to use DCE for a successful isolation of Au38.

Voltammetry studies on Au144 clusters showed that small, hydrophobic ions can penetrate the protecting monolayer on an oppositely charged nanoparticle and the extent of penetration was larger if the dielectric constant of the solvent was close to that of the monolayer.

Choosing the solvents and electrolytes for handling, electrochemical measurements and applications is an important factor. Chlorobenzene was shown to be preferable if the aim is to reduce monolayer desorption from Au38 resulting in stability in electrochemical measurements and long term storage. However, dichloroethane is the solvent of choice if the aim is to reduce ion penetration to the monolayer or to extract Au38 from larger clusters. Larger electrolyte ions did not penetrate the monolayer and therefore did not affect the charging signature. If such an electrolyte is used in electrochemical measurements, chlorobenzene would clearly be more preferable as the clusters are more stable and the solvent is also less toxic.

A method for building molecular surface density gradients and as a result, gradients of gold nanoparticles on surfaces was presented. The molecular area density on surface was controlled by varying the parameters on e-beam patterning of an aminosilane layer on silicon. The nanoparticle density reflecting the amino group density on the surface was shown to depend on the e-beam dose with larger dose resulting in lower nanoparticle density.

The results of the thesis are relevant for fundamental understanding of monolayer protected clusters as well as their practical handling. Improved characterization methods resolve the challenges in distinguishing small cluster sizes from each other. Reliable synthesis and characterization methods are a prerequisite for applications of these materials. Solvent dispersion is a crucial step in all practical handling of the clusters. The results can be applied when choosing conditions such as solvents or electrolytes for preparation, isolation, purification, storage and electrical applications. The nanoparticle gradient preparation method presented here can be used to prepare such structures of various types of materials in flexible geometries, dimensions and steepness. Surface attachment and gradient preparation is of interest in nanotechnology applications in the fields of electronics, sensing or biology.

References

1. Daniel, M.-C., Astruc, D., *Chem. Rev.* **104** (2004) 293.
2. Hutchings, G.J., Brust, M., Schmidbaur, H., *Chem. Soc. Rev.* **37** (2008) 1759.
3. Faraday, M., *Philos. Trans.* **147** (1857) 145.
4. Brust, M., Walker, M., Bethell, D., Schiffrin, D.J., Whyman, R., *J. Chem. Soc., Chem. Commun.* (1994) 801.
5. Murray, R.W., *Chem. Rev.* **108** (2008) 2688.
6. Nuzzo, R.G., Allara, D.L., *J. Am. Chem. Soc.* **105** (1983) 4481.
7. Haruta, M., Kobayashi, T., Sano, H., Yamada, N., *Chem. Lett.* (1987) 405.
8. Jain, P.K., El-Sayed, I.H., El-Sayed, M.A., *Nano Today* **2** (2007) 18.
9. Kamat, P.V., *J. Phys. Chem. C* **111** (2007) 2834.
10. Schmid, G., Corain, B., *Eur. J. Inorg. Chem.* (2003) 3081.
11. Schmid, G., Pfeil, R., Boese, R., Brandermann, F., Meyer, S., Calis, G.H.M., Van der Velden, J.W.A., *Chem. Ber.* **114** (1981) 3634.
12. Alvarez, M.M., Khoury, J.T., Schaaff, T.G., Shafigullin, M.N., Vezmar, I., Whetten, R.L., *J. Phys. Chem. B* **101** (1997) 3706.
13. Bowman, M.-C., Ballard, T.E., Ackerson, C.J., Feldheim, D.L., Margolis, D.M., Melander, C., *J. Am. Chem. Soc.* **130** (2008) 6896.
14. Turkevich, J., Stevenson, P.C., Hillier, J., *Discuss. Faraday Soc.* **11** (1951) 55.
15. Templeton, A.C., Wuelfing, W.P., Murray, R.W., *Acc. Chem. Res.* **33** (2000) 27.
16. Schaaff, T.G., Shafigullin, M.N., Khoury, J.T., Vezmar, I., Whetten, R.L., Cullen, W.G., First, P.N., Wing, C., Ascensio, J., Yacaman, M.J., *J. Phys. Chem. B* **101** (1997) 7885.
17. Hostetler, M.J., Wingate, J.E., Zhong, C.-J., Harris, J.E., Vachet, R.W., Clark, M.R., Londono, J.D., Green, S.J., Stokes, J.J., Wignall, G.D., Glish, G.L., Porter, M.D., Evans, N.D., Murray, R.W., *Langmuir* **14** (1998) 17.
18. Alvarez, M.M., Khoury, J.T., Schaaff, T.G., Shafigullin, M., Vezmar, I., Whetten, R.L., *Chem. Phys. Lett.* **266** (1997) 91.

19. Schaaff, T.G., Whetten, R.L., *J. Phys. Chem. B* **103** (1999) 9394.
20. Shimizu, T., Teranishi, T., Hasegawa, S., Miyake, M., *J. Phys. Chem. B* **107** (2003) 2719.
21. Qian, H., Zhu, M., Andersen, U.N., Jin, R., *J. Phys. Chem. A* **113** (2009) 4281.
22. Whetten, R.L., Khoury, J.T., Alvarez, M.M., Murthy, S., Vezmar, I., Wang, Z.L., Stephens, P.W., Cleveland, C.L., Luedtke, W.D., Landman, U., *Adv. Mater.* **8** (1996) 428.
23. Jimenez, V.L., Georganopoulou, D.G., White, R.J., Harper, A.S., Mills, A.J., Lee, D., Murray, R.W., *Langmuir* **20** (2004) 6864.
24. Donkers, R.L., Lee, D., Murray, R.W., *Langmuir* **20** (2004) 1945.
25. Lee, D., Donkers, R.L., Wang, G., Harper, A.S., Murray, R.W., *J. Am. Chem. Soc.* **126** (2004) 6193.
26. Negishi, Y., Nobusada, K., Tsukuda, T., *J. Am. Chem. Soc.* **127** (2005) 5261.
27. Zhu, M., Lanni, E., Garg, N., Bier, M.E., Jin, R., *J. Am. Chem. Soc.* **130** (2008) 1138.
28. Tracy, J.B., Kalyuzhny, G., Crowe, M.C., Balasubramanian, R., Choi, J.-P., Murray, R.W., *J. Am. Chem. Soc.* **129** (2007) 6706.
29. Wu, Z., Suhan, J., Jin, R., *J. Mater. Chem.* **19** (2009) 622.
30. Shichibu, Y., Negishi, Y., Tsunoyama, H., Kanehara, M., Teranishi, T., Tsukuda, T., *Small* **3** (2007) 835.
31. Kim, J., Lema, K., Ukaigwe, M., Lee, D., *Langmuir* **23** (2007) 7853.
32. Negishi, Y., Chaki, N.K., Shichibu, Y., Whetten, R.L., Tsukuda, T., *J. Am. Chem. Soc.* **129** (2007) 11322.
33. Chaki, N.K., Negishi, Y., Tsunoyama, H., Shichibu, Y., Tsukuda, T., *J. Am. Chem. Soc.* **130** (2008) 8608.
34. Dass, A., *J. Am. Chem. Soc.* **131** (2009) 11666.
35. Hicks, J.F., Miles, D.T., Murray, R.W., *J. Am. Chem. Soc.* **124** (2002) 13322.
36. Miles, D.T., Murray, R.W., *Anal. Chem.* **75** (2003) 1251.
37. Quinn, B.M., Liljeroth, P., Ruiz, V., Laaksonen, T., Kontturi, K., *J. Am. Chem. Soc.* **125** (2003) 6644.
38. Shon, Y.-S., Dawson, G.B., Porter, M., Murray, R.W., *Langmuir* **18** (2002) 3880.

39. Qian, H., Zhu, Y., Jin, R., *ACS Nano* **3** (2009) 3795.
40. Balasubramanian, R., Guo, R., Mills, A.J., Murray, R.W., *J. Am. Chem. Soc.* **127** (2005) 8126.
41. Schaaff, T.G., *Anal. Chem.* **76** (2004) 6187.
42. Schaaff, T.G., Shafigullin, M.N., Khoury, J.T., Vezmar, I., Whetten, R.L., *J. Phys. Chem. B* **105** (2001) 8785.
43. Tsunoyama, H., Negishi, Y., Tsukuda, T., *J. Am. Chem. Soc.* **128** (2006) 6036.
44. Tsunoyama, H., Nickut, P., Negishi, Y., Al-Shamery, K., Matsumoto, Y., Tsukuda, T., *J. Phys. Chem. C* **111** (2007) 4153.
45. Terrill, R.H., Postlethwaite, T.A., Chen, C.-h., Poon, C.-D., Terzis, A., Chen, A., Hutchison, J.E., Clark, M.R., Wignall, G., Londono, J.D., Superfine, R., Falvo, M., Johnson, C.S.J., Samulski, E.T., Murray, R.W., *J. Am. Chem. Soc.* **117** (1995) 12537.
46. Tracy, J.B., Crowe, M.C., Parker, J.F., Hampe, O., Fields-Zinna, C.A., Dass, A., Murray, R.W., *J. Am. Chem. Soc.* **129** (2007) 16209.
47. Jadzinsky, P.D., Calero, G., Ackerson, C.J., Bushnell, D.A., Kornberg, R.D., *Science* **318** (2007) 430.
48. Fields-Zinna, C.A., Sardar, R., Beasley, C.A., Murray, R.W., *J. Am. Chem. Soc.* **131** (2009) 16266.
49. Häkkinen, H., Walter, M., Grönbeck, H., *J. Phys. Chem. B* **110** (2006) 9927.
50. Walter, M., Akola, J., Lopez-Acevedo, O., Jadzinsky, P.D., Calero, G., Ackerson, C.J., Whetten, R.L., Grönbeck, H., Häkkinen, H., *Proc. Natl. Acad. Sci. U. S. A.* **105** (2008) 9157.
51. Heaven, M.W., Dass, A., White, P.S., Holt, K.M., Murray, R.W., *J. Am. Chem. Soc.* **130** (2008) 3754.
52. Zhu, M., Aikens, C.M., Hollander, F.J., Schatz, G.C., Jin, R., *J. Am. Chem. Soc.* **130** (2008) 5883.
53. Akola, J., Walter, M., Whetten, R.L., Häkkinen, H., Grönbeck, H., *J. Am. Chem. Soc.* **130** (2008) 3756.
54. Jiang, D., Luo, W., Tiago, M.L., Dai, S., *J. Phys. Chem. C* **112** (2008) 13905.
55. Pei, Y., Gao, Y., Zeng, X.C., *J. Am. Chem. Soc.* **130** (2008) 7830.

56. Lopez-Acevedo, O., Tsunoyama, H., Tsukuda, T., Häkkinen, H., Aikens, C.M., *J. Am. Chem. Soc.* **132** (2010) 8210.
57. Qian, H., Eckenhoff, W.T., Zhu, Y., Pintauer, T., Jin, R., *J. Am. Chem. Soc.* **132** (2010) 8280.
58. Lopez-Acevedo, O., Akola, J., Whetten, R.L., Grönbeck, H., Häkkinen, H., *J. Phys. Chem. C* **113** (2009) 5035.
59. Dass, A., Stevenson, A., Dubay, G.R., Tracy, J.B., Murray, R.W., *J. Am. Chem. Soc.* **130** (2008) 5940.
60. Henglein, A., *J. Phys. Chem.* **83** (1979) 2209.
61. Kiwi, J., Grätzel, M., *J. Am. Chem. Soc.* **101** (1979) 7214.
62. Green, S.J., Stokes, J.J., Hostetler, M.J., Pietron, J., Murray, R.W., *J. Phys. Chem. B* **101** (1997) 2663.
63. Ingram, R.S., Hostetler, M.J., Murray, R.W., Schaaff, T.G., Khoury, J., Whetten, R.L., Bigioni, T.P., Guthrie, D.K., First, P.N., *J. Am. Chem. Soc.* **119** (1997) 9279.
64. Chen, S., Ingram, R.S., Hostetler, M.J., Pietron, J.J., Murray, R.W., Schaaff, T.G., Khoury, J.T., Alvarez, M.M., Whetten, R.L., *Science* **280** (1998) 2098.
65. Pietron, J.J., Hicks, J.F., Murray, R.W., *J. Am. Chem. Soc.* **121** (1999) 5565.
66. Templeton, A.C., Chen, S., Gross, S.M., Murray, R.W., *Langmuir* **15** (1999) 66.
67. Laaksonen, T., Ruiz, V., Liljeroth, P., Quinn, B.M., *Chem. Soc. Rev.* **37** (2008) 1836.
68. Antonello, S., Holm, A.H., Instuli, E., Maran, F., *J. Am. Chem. Soc.* **129** (2007) 9836.
69. Chi, L.F., Hartig, M., Drechsler, T., Schwaack, T., Seidel, C., Fuchs, H., Schmid, G., *Appl. Phys. A: Mater. Sci. Process.* **66** (1998) S187.
70. Zhang, H., Schmid, G., Hartmann, U., *Nano Lett.* **3** (2003) 305.
71. Kim, Y.-G., Garcia-Martinez, J.C., Crooks, R.M., *Langmuir* **21** (2005) 5485.
72. Stiles, R.L., Balasubramanian, R., Feldberg, S.W., Murray, R.W., *J. Am. Chem. Soc.* **130** (2008) 1856.
73. Wolfe, R.L., Balasubramanian, R., Tracy, J.B., Murray, R.W., *Langmuir* **23** (2007) 2247.

74. Wolfe, R.L., Murray, R.W., *Anal. Chem.* **78** (2006) 1167.
75. Chen, S., Sommers, J.M., *J. Phys. Chem. B* **105** (2001) 8816.
76. Branham, M.R., Douglas, A.D., Mills, A.J., Tracy, J.B., White, P.S., Murray, R.W., *Langmuir* **22** (2006) 11376.
77. Zamborini, F.P., Gross, S.M., Murray, R.W., *Langmuir* **17** (2001) 481.
78. Chen, S., Murray, R.W., Feldberg, S.W., *J. Phys. Chem. B* **102** (1998) 9898.
79. Hicks, J.F., Templeton, A.C., Chen, S., Sheran, K.M., Jasti, R., Murray, R.W., Debord, J., Schaaff, T.G., Whetten, R.L., *Anal. Chem.* **71** (1999) 3703.
80. Guo, R., Georganopoulou, D., Feldberg, S.W., Donkers, R., Murray, R.W., *Anal. Chem.* **77** (2005) 2662.
81. Su, B., Girault, H.H., *J. Phys. Chem. B* **109** (2005) 11427.
82. Garcia-Morales, V., Mafe, S., *J. Phys. Chem. C* **111** (2007) 7242.
83. Negishi, Y., Takasugi, Y., Sato, S., Yao, H., Kimura, K., Tsukuda, T., *J. Phys. Chem. B* **110** (2006) 12218.
84. Menard, L.D., Gao, S.-P., Xu, H., Twesten, R.D., Harper, A.S., Song, Y., Wang, G., Douglas, A.D., Yang, J.C., Frenkel, A.I., Nuzzo, R.G., Murray, R.W., *J. Phys. Chem. B* **110** (2006) 12874.
85. Yang, Y., Chen, S., *Nano Lett.* **3** (2003) 75.
86. Williams, D.B., Carter, C.B., *Transmission Electron Microscopy I Basics*, Plenum Press, New York 1996, 173.
87. Abad, J.M., Sendroiu, I.E., Gass, M., Bleloch, A., Mills, A.J., Schiffrin, D.J., *J. Am. Chem. Soc.* **129** (2007) 12932.
88. Bard, A.J., Faulkner, L.R., *Electrochemical Methods*, 2nd ed., John Wiley & Sons, Inc., 2001, 833.
89. Quinn, B.M., Liljeroth, P., Kontturi, K., *J. Am. Chem. Soc.* **124** (2002) 12915.
90. Unwin, P.R., Bard, A.J., *J. Phys. Chem.* **95** (1991) 7814.
91. Volkov, A.G., Deamer, D.W., eds. *Liquid-Liquid Interfaces, Theory and Methods*. 1996, CRC Press, Boca Raton, 421.
92. Taylor, G., Girault, H.H.J., *J. Electroanal. Chem. Interfacial Electrochem.* **208** (1986) 179.
93. Liljeroth, P., Quinn, B.M., Kontturi, K., *Electrochem. Commun.* **4** (2002) 255.

94. Quinn, B.M., Kontturi, K., *J. Am. Chem. Soc.* **126** (2004) 7168.
95. Love, J.C., Estroff, L.A., Kriebel, J.K., Nuzzo, R.G., Whitesides, G.M., *Chem. Rev.* **105** (2005) 1103.
96. Gorman, C.B., Biebuyck, H.A., Whitesides, G.M., *Langmuir* **11** (1995) 2242.
97. Bhat, R.R., Fischer, D.A., Genzer, J., *Langmuir* **18** (2002) 5640.
98. Bhat, R.R., Genzer, J., Chaney, B.N., Sugg, H.W., Liebmann-Vinson, A., *Nanotechnology* **14** (2003) 1145.
99. Genzer, J., Bhat, R.R., *Langmuir* **24** (2008) 2294.
100. Ruardy, T.G., Schakenraad, J.M., van der mei, H.C., Busscher, H.J., *Surf. Sci. Rep.* **29** (1997) 1.
101. Chaudhury, M.K., Whitesides, G.M., *Science* **256** (1992) 1539.
102. Krämer, S., Xie, H., Gaff, J., Williamson, J.R., Tkachenko, A.G., Nouri, N., Feldheim, D.A., Feldheim, D.L., *J. Am. Chem. Soc.* **126** (2004) 5388.
103. Zhu, T., Fu, X., Mu, T., Wang, J., Liu, Z., *Langmuir* **15** (1999) 5197.
104. Baker, B.E., Kline, N.J., Treado, P.J., Natan, M.J., *J. Am. Chem. Soc.* **118** (1996) 8721.
105. Morgenthaler, S., Lee, S., Zürcher, S., Spencer, N.D., *Langmuir* **19** (2003) 10459.
106. Iqbal, P., Critchley, K., Bowen, J., Attwood, D., Tunnicliffe, D., Evans, S.D., Preece, J.A., *J. Mater. Chem.* **17** (2007) 5097.
107. Efimenko, K., Genzer, J., *Adv. Mater.* **13** (2001) 1560.
108. Song, F., Cai, Y., Zhang Newby, B.-m., *Appl. Surf. Sci.* **253** (2006) 2393.
109. Geissler, M., Chalsani, P., Cameron, N.S., Veres, T., *Small* **2** (2006) 760.
110. Fuierer, R.R., Carroll, R.L., Feldheim, D.L., Gorman, C.B., *Adv. Mater.* **14** (2002) 154.
111. Jiang, L., Wang, W., Fuchs, H., Chi, L., *Small* **5** (2009) 2819.
112. Laaksonen, P., Kivioja, J., Paananen, A., Kainlauri, M., Kontturi, K., Ahopelto, J., Linder, M.B., *Langmuir* **25** (2009) 5185.
113. Han, M., Xu, C., Zhu, D., Yang, L., Zhang, J., Chen, Y., Ding, K., Song, F., Wang, G., *Adv. Mater.* **19** (2007) 2979.

114. Werts, M.H.V., Lambert, M., Bourgoin, J.-P., Brust, M., *Nano Lett.* **2** (2002) 43.

115. Harnett, C.K., Satyalakshmi, K.M., Craighead, H.G., *Appl. Phys. Lett.* **76** (2000) 2466.

116. Harnett, C.K., Satyalakshmi, K.M., Craighead, H.G., *Langmuir* **17** (2001) 178.

117. Krupke, R., Malik, S., Weber, H.B., Hampe, O., Kappes, M.M., von Loehneysen, H., *Nano Lett.* **2** (2002) 1161.

118. Lercel, M.J., Redinbo, G.F., Pardo, F.D., Rooks, M., Tiberio, R.C., Simpson, P., Craighead, H.G., Sheen, C.W., Parikh, A.N., Allara, D.L., *J. Vac. Sci. Technol.* **12** (1994) 3663.

119. Mendes, P.M., Jacke, S., Critchley, K., Plaza, J., Chen, Y., Nikitin, K., Palmer, R.E., Preece, J.A., Evans, S.D., Fitzmaurice, D., *Langmuir* **20** (2004) 3766.

120. Mendes, P.M., Preece, J.A., *Curr. Opin. Colloid Interface Sci.* **9** (2004) 236.

121. Sondag-Huethorst, J.A.M., van Helleputte, H.R.J., Fokkink, L.G.J., *Appl. Phys. Lett.* **64** (1994) 285.

122. Weimann, T., Geyer, W., Hinze, P., Stadler, V., Eck, W., Gölzhauser, A., *Microelectron. Eng.* **57-58** (2001) 903.

123. Ballav, N., Shaporenko, A., Krakert, S., Terfort, A., Zharnikov, M., *J. Phys. Chem. C* **111** (2007) 7772.

124. Ballav, N., Shaporenko, A., Terfort, A., Zharnikov, M., *Adv. Mater.* **19** (2007) 998.

Errata

In Publication I, in Table 1, the extent of ion penetration (α) for PF_6^- in CB should be 0.9-0.44, not 0.35, and correspondingly, the (a_1-r_0) values should be 6.9-3.4. The ionic radius used for PF_6^- was 1.4, not 1.8. The values are correct in the article text and in the thesis.

Gold nanoparticles are a fascinating research topic due to their optical, electronic, catalytic and biological applications. They are the most stable nanoparticles and provide a basis to study nanoscale phenomena. The ability to prepare a specific size, reliably characterize the product and controllably attach the particles on surfaces is important when considering the applications.
Electrochemical methods are used to characterize thiolate-protected gold clusters with diameters smaller than 2 nm as well as to study their stability, reaction mechanisms and the interaction of the stabilizing thiolate layer with the environment. This thesis reports recent developments in synthesis and characterization of clusters with diameters in the order of 1 nm, density control of nanoparticles on surfaces, and the use of electrochemical methods in the field. The results are relevant for fundamental understanding, practical handling and choosing the conditions for applications of gold nanoparticles.

Aalto-DD 19/2011

ISBN: 978-952-60-4057-8 (pdf)
ISBN: 978-952-60-4056-1
ISSN-L: 1799-4934
ISSN: 1799-4942 (pdf)
ISSN: 1799-4934

Aalto University
School of Chemical Technology
Department of Chemistry
aalto.fi

BUSINESS + ECONOMY

ART + DESIGN + ARCHITECTURE

SCIENCE + TECHNOLOGY

CROSSOVER

DOCTORAL DISSERTATIONS